Major routes in the photocatalytic methane conversion into chemicals and fuels under mild conditions

Vitaly Ordomsky, Songwei Zhang, Jerry Pui Ho Li, Jingpeng Zhao, Dan Wu, Biao Yuan, Willinton Yesid Hernández, Wen-Juan Zhou, Tao He, Yi Yu, et al.

Version of Record: https://www.sciencedirect.com/science/article/pii/S0926337321000394
Manuscript_deb2acd8cf82c075d1314c0e9dab5ce9

Revised on January 2nd, 2021

Major routes in the photocatalytic methane conversion into chemicals and fuels under mild conditions

Di Hu, Vitaly V. Ordomsky and Andrei Y. Khodakov**

University of Lille, CNRS, Centrale Lille, University of Artois, UMR 8181 – UCCS – Unité de Catalyse et Chimie du Solide, Lille, France

Corresponding authors: vitaly.ordomsky@univ-lille.fr; andrei.khodakov@univ-lille.fr

Abstract

Methane is one of the most abundant molecules on Earth. Most of the state-of-the-art methane chemical conversion technologies require high temperatures, they are accompanied by insufficient selectivity, carbon deposition and major production of carbon dioxide. Development of the methane conversion technologies at mild conditions is important for the rational utilization of renewable and fossil feedstocks and for the environment.

The goal of this review is to perform a comparative analysis of low temperature methane photocatalytic conversion routes such as methane oxidation, methane reforming and methane coupling. Methane photocatalytic reforming currently exhibits the highest conversion rate, while methane coupling shows the highest selectivity. The most promising routes could be methane oxidation to methanol, which simultaneously exhibits higher productivity and selectivity. Further improvements in the methane conversion can be achieved by the design of new materials, photoreactors and operating modes, such as photochemical looping and combining photocatalysis with electrocatalysis.

Keywords: methane; activation; photocatalysis; mild conditions; methanol

1. Introduction

1.1 Vast and diverse methane feedstocks

Methane comes from renewable and fossil resources: biogas, natural gas, coal gas, shale gas and clathrates in the ocean floors. In recent years, abundant feedstocks of unconventional shale gas, coalbed gas and tight gas have doubly overwhelmed the proven conventional natural gas reserves [1]. Methane is an important source of energy. It is used as a fuel for electricity generation, industry, heating and transport. Methane combustion corresponds to 20-25% of the global emission of carbon dioxide. Significant amounts of methane are nowadays burned out at the oil production sites. Methane "flaring" consumes 3.5 % of the global natural gas production. Methane is itself a greenhouse gas (GHG) with an effect 30 times higher than carbon dioxide. In terms of warming potential, methane global emissions to the atmosphere since 2000, correspond to putting 350 million more cars on the world's roads. Methane is also involved in the ground-level formation of ozone, which is an air pollutant and bad for human health. Elaboration of new sustainable technologies of methane chemical conversion can, therefore, solve both the problems of rational utilization of fossil and renewable resources and address the global warming and environmental concerns.

1.2. State of the art methane conversion

The state-of-the-art chemical conversion (**Figure 1**) can be divided into direct and indirect routes [2–4]. In the indirect methane conversion, methane is first transformed to syngas (a mixture of carbon monoxide and hydrogen) and then syngas is used in numerous processes such as methanol synthesis, Fischer-Tropsch reaction, hydroformylation, hydrogen production etc. The indirect conversion of methane to fuels and chemicals via intermediate formation of syngas currently corresponds to large industrial units. The conventional methane

indirect conversion technologies include steam reforming of methane (SRM), partial oxidation of methane (POM), autothermal reforming (ATR) and dry reforming of methane (DRM).

SRM (Eq. 1) is an endothermic reaction, which has been effectively performed at high temperatures (above 800 °C) and pressures between 2 and 3.5 MPa:

$$CH_4 + H_2O\ (g) \rightarrow CO + 3H_2,\ \Delta H^0_{298K} = 205.9\ kJ \cdot mol^{-1} \quad (1)$$

The process yields syngas with the H_2/CO ratio of about 3, which is too high for either Fischer-Tropsch or methanol synthesis. SRM in combination with the water gas shift reaction (WGS, $H_2O+CO \rightarrow H_2+CO_2$) is also employed for industrial hydrogen production. Currently, 95% of the world's hydrogen is produced by SRM. The process is generally carried out in large multi-tubular fixed-bed reactors with supported nickel catalysts.

In POM, methane is oxidized to syngas with a sub-stoichiometric amount of oxygen either with or without catalyst:

$$CH_4 + 1/2O_2 \rightarrow CO + 2H_2,\ \Delta H\ ^0_{298K} = -36\ kJ\ mol^{-1} \quad (2)$$

The non-catalytic POM typically requires harsh conditions and high temperature (T>1200°C) and is often accompanied by undesired methane combustion, while the catalytic POM operates efficiently in the range of 750-950 °C and pressure of 2.5-3.5 MPa. The exothermicity of POM may lead to the formation of hot spots inside the reactor. The use of oxygen for POM presents nonnegligible risks of explosion and catalyst oxidation. The ATR process, which represents a combination of SRM and POM, is performed at temperatures above 850 °C and pressure of 0.1-8 MPa.

In addition to the industrial syngas production processes, DRM (Eq. 3) is considered as a potential alternative to simultaneously convert two greenhouse gases (methane and carbon dioxide) into syngas with the H_2/CO ratio of about 1. DRM is generally carried out at ambient pressure and temperature higher than 800 °C.

$$CH_4+CO_2 \rightarrow 2\,H_2 + 2\,CO,\ \Delta H^{0}_{298K} = 247 kJ/mol \quad (3)$$

Huge energy requirement, coke deposition and catalyst sintering are three main thorny problems of DRM.

The direct methane conversion [2] includes (**Figure 1**) non-oxidative (NOCM) and oxidative coupling of methane (OCM), partial oxidation of methane (POM) to oxygenates, methane aromatization, oxidative Andrussow and non-oxidative BMA (or Degussa) processes. Among direct methane conversion routes, only the Andrussow (Eq. 4) and BMA (Eq. 5) processes, which produce hydrogen cyanide, have been commercialized[5]:

$$CH_4 + NH_3 + 3/2O_2 \rightarrow 3H_2O + HCN,\ \Delta H^{0}_{298K} = -483\ kJ\cdot mol^{-1} \quad (4)$$

$$CH_4 + NH_3 \rightarrow 3H_2 + HCN,\ \Delta H^{0}_{298K} = 251\ kJ\cdot mol^{-1} \quad (5)$$

Thermodynamic limitations hinder direct nonoxidative methane coupling to the C_2 hydrocarbons. The coupling reaction requires extremely high temperatures, generates aromatics as byproducts and is accompanied by rapid carbon deposition. The exothermic oxidative coupling of methane (OCM, Eq. 6) with oxidants (such as oxygen, water and N_2O) can be performed at 750-950 °C:

$$2CH_4 + O_2 \rightarrow C_2H_4 + 2H_2O,\ \Delta H^{0}_{298K} = -280\ kJ\cdot mol^{-1} \quad (6)$$

Production of major amounts of undesirable carbon dioxide and carbon deposition over catalysts are major drawbacks of both the NOCM and OCM reactions. None of the developed catalysts and processes have fulfilled so far the industrial demands in terms of selectivity, conversion and stability [2].

Methane catalytic aromatization (Eq. 7) is also an extremely thermodynamically unfavorable reaction [6]:

$$6CH_4 \rightarrow C_6H_6 + 9H_2,\ \Delta H^{0}_{298K} = 531\ kJ\cdot mol^{-1} \quad (7)$$

The maximum thermodynamically possible benzene yield of about 12% can be obtained at 700 °C. Though the addition of hydrogen or oxidants (O_2, CO, CO_2, NO and

steam) may limit carbon formation, the major barriers for its practical application are insufficient selectivity and inevitable overoxidation of reaction products in the presence of oxidizing agents (**Figure 2**).

The direct methane oxidation to the C_1 oxygenates (methanol, formaldehyde or formic acid) has been widely studied in both gaseous and liquid phases on various catalytic systems. The oxygenates generated in direct methane oxidation can be more easily over-oxidized to carbon dioxide than methane. A wide range of oxidants have been involved in this process, such as O_2, N_2O, H_2O_2 and even water. It was shown that H_2O_2 might elevate [7–10] the selectivity of methane oxidation toward methanol and can be used at relatively mild conditions. Recently, binuclear [11] and trinuclear [12] copper oxo-clusters in zeolites have shown noticeable activity in the methane oxidation to methanol. Because of thermodynamic limitations [13–15], the reaction has to be performed using chemical looping and temperature swings. Formaldehyde is another possible product of POM. The best reported results [2] correspond, however, to the maximum formaldehyde selectivity of 50% at the methane conversion below 3%.

1.3. Challenges in methane chemical conversion

The state of state-of-the-art methane direct or indirect chemical conversion suffers from the following shortcomings:

- high energy consumption, which is required to conduct the methane conversion at high temperatures or to use temperature and pressure swings in the chemical looping processes;
- insufficient selectivities to the target products and emission of large amounts of carbon dioxide;

- rapid catalyst deactivation at high reaction temperatures in both oxidizing and non-oxidizing atmospheres, due to extensive carbon deposition and catalyst sintering;
- thermodynamic limitations for the methane conversion in the absence of oxidizing agents.

In order to improve the efficiency of methane conversion, two main challenges should be considered: methane activation and instability of the reaction intermediates and products. The high energy consumption associated with the methane conversion should be addressed by conducting the reaction at mild conditions and if possible, even at ambient temperature [16–18]. In the low temperature processes, the energy for methane activation can be provided either by the external energy (light, electricity) or by the reacting agents with high energy density, such as oxygen, hydrogen peroxide.

Methane is an extremely inert molecule. Methane activation has been for a long time a "holy grail" [3,17,19,20] of modern science. The C-H bond energy of methane is about 434 $kJ \cdot mol^{-1}$ (4.5 eV), which is the highest among all alkanes. The chemical stability of methane is also closely related to the symmetric tetrahedral molecular geometry, which leads to low polarizability, weak acidity and low affinity for electrons and protons. Most of the products of methane conversion (ethane, ethylene, methanol, formaldehyde, formic acid, carbon monoxide etc.) are more reactive than methane. This results in their overoxidation and reduces the selectivities to the target products. Consequently, the methane conversion is usually accompanied by the production of large amounts of more stable and kinetically inert carbon dioxide and carbon (**Figure 2**).

1.4. Photocatalysis

Solar energy, which is cheap, non-polluting and abundant, provides a potential way to solve both environmental and energy challenges of methane activation and conversion.

Photocatalysis, converting the light energy into chemical energy of various chemicals, could occur at mild conditions and under ambient temperature [17,21–23].

Photocatalysts refer to a class of semiconductor materials that can induce photocatalytic redox reactions upon irradiation. In general, heterogeneous photocatalysts can be divided into two main categories. The first category is the bulk semiconductor photocatalysts, such as TiO_2, ZnO, CdS, and WO_3 [24]. The second category is supported or highly dispersed photocatalysts, such as Pd/TiO_2 [25], MgO/TiO_2 [26], TiO_2/SiO_2 [27], and La/WO_3 [28].

The semiconductor (**Figure 3**) is characterized by its electronic band structure constituted of the valence band (VB) and conduction band (CB). The VB electrons firstly absorb incident light with energy equivalent or/and exceeding the bandgap, resulting in charge transfer from VB to CB. The electrons (e^-) and holes (h^+), also called photogenerated charge carriers, are formed in VB and CB, respectively, and then migrate to the surface of photocatalytic materials (**Figure 3**). Subsequently, the interaction of the photogenerated charge carriers with reacting molecules strongly depends on their redox potential and energies of the conduction band minimum (CBM) and valence band maximum (VBM) [29]. The lifetime of the photogenerated charge carriers is also a critical characteristic determining the photocatalytic efficiency. The electron–hole pairs usually have a lifetime of about 10^{-9} s, while the chemical process requires between 10^{-8} and 10^{-3} s. Most of photogenerated charge carriers undergo recombination processes on the surface and/or in the volume or can be captured by the defect sites in semiconductors, releasing the recombination energy as heat or photons. This inevitably decreases the availability of photogenerated charge carriers for the photoactivation of reacting molecules. The recombination of the photo-excited electron-hole pairs should be, therefore, retarded.

In order to improve the optical-electrical characteristics of photocatalytic materials, many studies have been focused on the engineering of semiconductor electronic band

structure and narrowing the bandgap in order to conduct the reactions under visible light. Moreover, there have also been numerous works to lengthen the lifetime of photogenerated charge carriers by promoting charge separation and accelerating charge transfer by doping of photocatalysts, building heterojunctions, addition of metal nanoparticles, quantum dots and electron scavengers. Doping with different elements has been shown to be efficient in narrowing the bandgap, extending the light absorption of photocatalytic materials into longer wavelengths or even into the visible light region. The heterojunction formed between two semiconductors limits the movement of photogenerated charge carriers, retards their recombination and facilitates charge separation [30–32]. The type II and Z-scheme are heterojunctions commonly described [33]. In the type-II heterojunctions, the improved charge-separation efficiency coincides with a narrower range of potential variations for the redox reactions. The indirect and direct Z-scheme heterojunctions suffer disadvantages such as solution phase limitation, side reactions and light shielding. Recently, the S-scheme heterojunction mechanism has been proposed [33] (**Figure 4**), which overcomes the drawbacks of the conventional II type and Z-scheme heterojunctions [33]. Similar to type-II heterojunction, the S-scheme heterojunction is composed of reducing and oxidizing photocatalysts with staggered band structures. In the S-scheme heterojunction, high energy photogenerated electrons in the conduction band of reducing photocatalysts and holes in the valence band of oxidizing photocatalysts have extended lifetime, while the recombination of the photoelectrons in the conduction band of oxidative photocatalysts and in the valence band of reducing photocatalyst has been enhanced. The S-scheme heterojunction provides an opportunity to conduct the photocatalytic reactions with a broader range of oxidizing and reducing potentials.

Addition of metal nanoparticles (Pt, Au, Ag and Ru [34,35]) results in significant improvement of photocatalytic performance. The Schottky barriers formed between the

intimate interface of metal nanoparticles and semiconductors favor separation and transfer of photogenerated charge carriers to active sites. Besides, metal nanoparticles can also operate as co-catalysts for the photocatalytic reactions [36,37]. The most efficient are usually noble metals. Rarity and high prices restrict, however, the extensive application of noble metals for photocatalysis. Finally, adding electron scavengers such as Fe^{3+}, Cu^{2+}, Ag^{+} or H_2O_2 is also helpful for the separation and transfer of photogenerated charge carriers, thus enhancement of the photocatalytic efficiency [38].

Under UV and/or visible light irradiation, some particular metal nanostructures, such as Au [39], Ag [40], Cu [41] and Ni [42] nanoparticles, show a localized surface plasmon resonance (LSPR) accompanied with significantly enhanced light absorption. LSPR is the collective free electron charge oscillation in the metallic nanoparticles that are excited by light [43]. It results in a strong electromagnetic field around metal particles and accelerates charge separation and forms energetic hot electrons and hot holes. Moreover, the decay of hot electrons brings significant thermal effect upon plasmonic metal nanostructures [44]. The intensity and resonance wavelength of LSPR over plasmonic metal nanostructures are tunable by modifying their morphology and particle size. Temperature is especially significant for the photocatalysts with the LSPR metals. The real surface temperature over the LSPR metals can be significantly higher [45–47] compared to the average temperature in the photoreactor.

The photocatalytic reactions may have rather complex mechanisms and usually involve several elementary steps and intermediates. These reaction steps can be affected by different extent by charge separation, migration and lifetime. The overall selectivity of methane conversion is a function of the rate of these different steps and would be affected by the presence of co-catalysts.

The performance of photocatalysts principally depends on the following characteristics:

- Band gap energy;

- Energy position of the conduction band minimum (CBM) and valence band maximum (VBM);
- Life time of electrons and holes;
- Presence of a co-catalyst.

In the last decades, photocatalysis has been shown to be very promising for water decomposition and environmental remediation. Since a few years, a large number of publications have addressed photocatalytic reduction of carbon dioxide. Recently, photocatalysis has also demonstrated a great potential for the selective methane conversion to fuels and chemicals occurring under mild conditions. The number of publications dedicated to photocatalytic methane conversion is exponentially growing in the last two decades **(Figure 5**).

2. Photocatalysis for selective methane conversion

One of the first stages of methane chemical conversion is its activation, requires a significant energy supply. Direct methane ionization or direct C-H bond cleavage in the gaseous methane both require very high energy, which is obviously impractical for real use. The role of any catalyst is, therefore, to reduce the activation energy of methane activation and to shift the reaction selectivity to a specific target product. In classical thermal catalysis, activation of the C-H bond in the methane molecule requires high temperature (>500 °C). In photocatalysis, the energy of photons provides an alternative energy source for methane activation, which may occur under irradiation even at room temperature. Photocatalysts, which decrease the energy of methane photocatalytic activation and enable efficient selective methane conversion at ambient temperatures under irradiation, are therefore considered as critical factors.

The C-H bond cleavage is usually strongly associated with the generation of the reaction intermediates upon light irradiation [48]. There have been generally two main mechanisms of methane photocatalytic activation [17]. The first mechanism involves the formation of electrophilic oxygen-centered radicals (such as O^-, OH•, •O-R, etc.), which react with methane and which abstract a H atom from methane. The activation barriers for abstracting a H atom and for the methane activation are lowered in this way [49]. The second mechanism considers the metal-CH_3 species as the reaction intermediates. These species form via methane dissociation over a photocatalyst.

The goal of our review is to perform a comparative and extensive analysis of methane photocatalytic conversion occurring at mild conditions and often at ambient temperature. More specifically, we consider three methane photocatalytic conversion routes: partial oxidation, reforming and coupling. Detailed information about the reaction conditions, productivity and selectivity of methane photocatalytic oxidation, reforming and coupling is given respectively in **Tables S1, S2 and S3** (**SM**). The methane photocatalytic reactions are discussed together and compared using quantitative criteria such as selectivity to the target products and productivity. We will also address the scientific maturity, which provides an estimate of state-of-the-art understanding of the phenomena occurring during methane conversion at both molecular and technological levels and perspectives for further scientific and technological breakthroughs. The analysis of current trends in the chemistry and catalysis of methane photocatalytic activation and conversion is principally performed based on the literature published in the last 10 years.

2.1. Photocatalytic methane oxidation

The partial oxidation of methane (POM) provides an opportunity for direct selective production of various value-added chemicals. Very often, methanol is the target product of

methane photocatalytic oxidation. In addition, complete oxidation of methane (COM) to carbon dioxide is also considered as a promising approach for reducing global warming. Methane is a greenhouse gas with a potential 30 times higher than that of CO_2 and can be present in small amounts in the atmosphere. It can be expected, therefore, that COM could reduce global warming. Titania [50] and zinc oxide [51] promoted with silver nanoparticles showed a good photocatalytic activity in methane complete oxidation. The photocatalysis can therefore clean [52] the atmosphere from non-CO_2 GHGs such as methane, reduce the global warming effect and simultaneously generate renewable electricity.

Molecular oxygen is prevalent among all the oxidants for the photocatalytic methane oxidation, due to its easy availability and economic superiority. Various O radicals formed from molecular oxygen under irradiation play an important role in methane activation and conversion. In the pioneering work, Kazansky et al. [53] studied reactions of methane with the photogenerated hole centers over TiO_2 and V/SiO_2 in the presence and absence of molecular oxygen under UV irradiation at mild temperature. The methane conversion resulted in the production of formaldehyde, ethane and CO_x. It was revealed that the photogenerated O^- hole centers were consumed in the absence of oxygen. They were responsible for the formation of methyl radicals and alkoxide intermediate species (CH_3O^- and $C_2H_5O^-$), while the surface ions Ti^{4+} and V^{5+} were simultaneously reduced by electrons. In the presence of oxygen, both COM and POM were enhanced, but POM was predominant. Additional oxygen was suggested to easily trap free electrons and formed more active oxygen species. Moreover, oxygen also played a key role in hindering metal reduction, which caused catalyst deactivation. Similarly, the O^- radicals of transition metal oxides, such as WO_3, V_2O_5, ZnO and MoO_3, played an important role in methane oxidation. Chen and co-workers [54] reported that the nano-scaled zinc oxide effectively oxidized methane in the presence of oxygen under UV-visible light at ambient conditions. The photogenerated surface O^- species and molecular oxygen were

responsible for the formation of formaldehyde intermediates and for the complete oxidation to carbon dioxide. It was found that smaller zinc oxide nanoparticles favored the photocatalytic methane oxidation. Moreover, additional silver decoration further enhanced the catalytic performance due to the silver LSPR. Ward et al. [35] reported that MoO_3 catalyzed selective oxidation of methane into methanol in the presence of oxygen at 100 °C under UV irradiation. The authors suggested that the surface absorbed H_2O was possibly involved in methanol production through the methyl radical pathway. Furthermore, additional doping with the Cu^{2+} cations made the photocatalyst sensitive to the visible light, due to the narrowed O $2p \rightarrow$ Cu $3d$ excitations in $CuMoO_4$. The electron trapping capability of Cu^{2+} lengthened the lifetime of O^- radicals. Sastre and co-workers [55] discovered methane oxidation with molecular oxygen to the liquid C_1 oxygenates with the selectivity above 95% over zeolites at room temperature under deep UV irradiation. The methanol productivity was about 194 $\mu mol \cdot g_{cat}^{-1} \cdot h^{-1}$ with the selectivity of 40.5%. They suggested that upon irradiation the surface silyloxyl radicals (Si-O•) derived from surface silanol groups generated methyl radicals, and then further formed the silyl methyl ethers ($Si\text{-}OCH_3$). Their decomposition yielded methanol. Moreover, the pore structure played an important role in providing silanol groups and confined space for methane activation. The presence of oxygen was critical for determining the reaction pathway of methyl radicals, thus directly influenced the selectivity. Highly selective CH_3OH production was achieved [56] in aerobic photocatalytic CH_4 oxidation by $Au_{0.75}/ZnO$ at atmospheric temperature. The Au nanoparticles were involved in the plasmonic affect, maximizing the electron and hole utilization. Isotopic tests showed that CH_3OH was produced from the combination of the CH_3 radicals with either O_2 or OH•.

Recently, our group discovered that zinc-heteropolyacid-titania nanocomposites catalyzed selective oxidation of methane into carbon monoxide using a 300 W Xe lamp at ambient temperature in the presence of molecular oxygen [30]. The optimized Zn-HPW/TiO_2

nanocomposite exhibited a high carbon monoxide productivity of 429 $\mu mol \cdot g_{cat}^{-1} \cdot h^{-1}$ in the batch reactor containing 3 bar of methane and 1 bar of oxygen. It turned out that all the three TiO_2, HPW and Zn components of the nanocomposites were essential for selective carbon monoxide production. TiO_2 harvested photons and achieved charge separation, HPW then promoted the transfer of photogenerated charge carriers, and Zn thus provided efficient active sites in the form of the charge-transfer excited complex $[Zn^{+}–O^{-}]$ for the formation of methyl carbonate intermediates (**Figure 6**). The decomposition of methyl carbonate intermediates generated from the zinc carbonates produced carbon monoxide, and zinc was simultaneously reduced by electrons. We suggested that the lattice oxygen of nanocomposite mainly participated in the oxidation of methane, similar to the Mars-Van Krevelen mechanism, while the gaseous oxygen was critical for the continuous zinc oxidation-reduction cycling during the catalytic process.

Alternatively to molecular oxygen, other oxidants, such as NO, H_2O and H_2O_2 have thus been studied to selectively convert methane into various value-added oxygenates [38,57,58]. Hu and co-workers [57] discovered that V-MCM-41 selectively oxidized methane into methanol with the selectivity of 87.6% using NO as an oxidant at mild temperature under UV irradiation, . They suggested that the charge-transfer excited $[V^{4+}–O^{-}]$ species reacted with both methane and NO and produced methyl radicals and then methanol. Thus, the vanadium oxidation-reduction cycle produced methanol. The CO_2 production with selectivity of 98.7% was observed in the presence of oxygen.

Water was found to be very promising for methane selective oxidation. The promoting effect of water on methane activation is usually attributed to the formation of OH• radicals. Chen and Li [59] reported the methane oxidation over the water preabsorbed TiO_2 and Mo/TiO_2 at mild conditions under UV irradiation in the presence of oxygen with the methanol productivity of 12.5 $\mu mol \cdot g_{cat}^{-1} \cdot h^{-1}$.The dehydrated counterparts only produced CO_x. It seems

that water could be a critical factor for selective oxidation of methane into methanol over some catalysts. Gondal et al. [60] studied methane oxidation induced by UV laser beam over the WO_3, TiO_2 and NiO semiconductors at room temperature in aqueous solution. The strong laser beam resulted in more effecient electron-hole excitation and water oxidation to hydroxyl radicals. This enhanced the methane conversion to above 20% over all samples. Among them, the maximum methanol productivity (529 $\mu mol \cdot g_{cat}^{-1} \cdot h^{-1}$) followed by a decrease with the irradiation time, was observed for WO_3, the decrease resulted from the methanol degradation in which a high concentration of methanol competitively donated electron to holes due to the band structure of WO_3. They further reported even higher methanol production rate over Ag impregnated WO_3 at room temperature under laser irradiation, in the presence of water [61]. The surface Ag^+ ions enhanced the formation of hydroxyl radicals by suppressing charge carrier recombination upon both the Ag_2O and WO_3 nanoparticles. However, besides the methanol degradation, the non-selective oxidation of excessive hydroxyl radicals also resulted in further methanol oxidation and produced a variety of by-products. Recently, Du et al. [62] discovered that in the presence of water, the CeO_2 nanoparticles calcined at high-temperatures selectively catalyzed methane oxidation into ethanol and aldehyde at ambient conditions under simulated solar light. The concentration of oxygen vacancies in the catalysts was critical for the formation of hydroxyl radicals upon irradiation, and a higher Ce^{III}/ Ce^{IV} ratio favored ethanol formation. The optimized CeO_2 nanoparticles achieved the ethanol productivity of 11.4 $\mu mol \cdot g_{cat}^{-1} \cdot h^{-1}$ with the selectivity of 91.5%. Zhu and co-workers [63] fabricated bipyramidal $BiVO_4$ and achieved methanol productivity (112 $\mu mol \cdot g_{cat}^{-1} \cdot h^{-1}$, selectivity over 85%) at mild temperature under simulated solar irradiation in the presence of water. The catalyst structures and proposed mechanism are shown in **Figure 7**, methanol was produced via the methyl radical pathway. The intermediate reactivity of exposed facets and easier formation of photoexcited holes in the bipyramid structure favored selective methane

oxidation, while the larger amount of CO_2 was detected over platelet-liked $BiVO_4$. Villa et al. [38] compared methane oxidation in various aqueous suspensions containing mesoporous WO_3 at mild temperature under UVC-visible light irradiation. The methanol production rate of 27.1 $\mu mol \cdot g_{cat}^{-1} \cdot h^{-1}$ with the selectivity of 46.2% was obtained in the presence of methane and pure water, while the presence of the Fe^{3+} electron scavenger in the aqueous solution increased the methanol production rate to 67.5 $\mu mol \cdot g_{cat}^{-1} \cdot h^{-1}$ with selectivity of 58.5%. It was proposed [64] that the addition of Fe^{3+} not only improved charge separation, which favored the production of $HO\bullet_{ads}$, but also enhanced production of free hydroxyl radicals via photolysis ($Fe^{3+} + H_2O \rightarrow Fe^{2+} + HO\bullet + H^+$). The H_2O_2 aqueous solutions have enhanced capability to provide abundant hydroxyl radicals [65]. For the WO_3 counterpart, in the presence of methane and H_2O_2 aqueous solution, the ethane production predominated instead of methanol. The formation of methanol was favored by adsorbed surface hydroxyl species , Thus the methyl radicals generated by free hydroxyl radicals mainly went for the methane coupling. The proposed mechanism was further confirmed in another work [66] (**Figure 8)**.

Xie and co-workers [58] discovered that an optimized FeO_x/TiO_2 nanocomposite consisted of highly dispersed iron species anchored on TiO_2 achieved methanol productivity of 1056 $\mu mol \cdot g_{cat}^{-1}$ with the selectivity over 90% at ambient conditions under simulated sunlight irradiation in the presence of H_2O_2, and only produced a trace amount of CO_x. They suggested that Fe^{3+} species not only improved the electron-hole separation, but also lowered the overpotential for H_2O_2 reduction, which avoided the formation of O_2^- and over-oxidation coincided with the formation of CO_2 (**Figure 9)**. The photoexcitation occurred upon TiO_2 and photogenerated holes were left in the VB of TiO_2 to form methyl radicals, while the photogenerated electrons were transferred to the surface iron species to participate in the H_2O_2 reduction with a lowered energy barrier.

Note that excessive generation of hydroxyl radicals or O_2^- from either H_2O_2 or H_2O would cause the undesired over-oxidation of products. It has thus been necessary to optimize the concentration of these oxidizing radicals for selective methane oxidation. Murcia-López and co-workers [67] uncovered a methanol production with the selectivity of 99.9% over $BiVO_4$ in the presence of nitrite ions in aqueous solution. The nitrite ions were suggested to behave as both the HO• scavengers and UV filters, thus inhibiting excessive formation of hydroxyl radicals. A significantly improved methanol selectivity has been achieved. Larger CO_2 production and smaller amount of C_2H_6 were observed in the $BiVO_4$ counterpart without nitrite ions in aqueous solution. Zhou and co-workers [68] discovered that copper modified polymeric carbon nitride (PCN) enabled highly selective production of alcohols at ambient temperature under visible light with the methanol and ethanol productivity of 24.5 $\mu mol \cdot g_{cat}^{-1} \cdot h^{-1}$ and 106 $\mu mol \cdot g_{cat}^{-1} \cdot h^{-1}$, respectively. The proper band structure of catalysts enabled the reaction of water and holes to generate H_2O_2, which then accomplished a catalytic cycle with the oxidation-reduction of the mixed-valence Cu species. They suggested that the synergy of the Cu species and adjacent C atoms in PCN played an essential role in ethanol generation. The in-situ decomposition of H_2O_2 over the Cu species largely avoided the disadvantage of excessive hydroxyl radical accumulation. Besides, Cu species also acted as active sites for methane activation.

2.2. Photocatalytic methane reforming

Steam reforming and dry reforming of methane (SRM and DRM) are promising ways to directly convert methane into valuable syngas, a mixture of carbon monoxide and hydrogen. Conventional methane reforming involves heterogeneous catalysts and requires higher temperatures. Thermocatalytic methane reforming is often accompanied by rapid catalyst deactivation due to sintering and carbon deposition. Photocatalytic methane reforming

occurring under mild conditions appears as a promising strategy, which can reduce energy consumption, improve the selectivity to CO and hydrogen and largely avoid coke formation and sintering.

2.2.1. Dry reforming of methane (DRM)

There have been so far several reports about the photocatalytic DRM process. Tanaka and co-workers [69,70] discovered that methane reacted with carbon dioxide over ZrO and MgO and selectively produced carbon monoxide under irradiation at room temperature. A very small amount of hydrogen was observed relative to carbon monoxide. The isotopic experiments uncovered that carbon monoxide originated from carbon dioxide instead of methane, while the methane conversion resulted in carbonaceous residues on the surface. The proposed mechanism [71] (**Figure 10**) suggests that carbon dioxide is firstly photoexcited to the $\bullet CO_2^-$ anion radicals, which then activate methane and form the surface acetate species and formate intermediates. The electron transfer to carbon dioxide is an energy consuming process and requires -1.9 eV [72], but it can be facilitated by the presence of water vapor [71]. $Cu/CdS–TiO_2/SiO_2$ was reported to selectively convert methane and carbon dioxide into acetone with selectivity of 92.3% under UV irradiation at the temperature of 120 °C [73]. The authors suggested that both methyl radicals and $\bullet CO_2^-$ anion radicals were responsible for the formation of acetone, while ethane and carbon monoxide were originated from methane and carbon dioxide, respectively. Yoshida and co-workers [74] discovered that both hydrogen and carbon monoxide were simultaneously produced via photocatalytic DRM under UV irradiation over Ga_2O_3. The mild reaction temperature of 200 °C was essential to drive the photocatalytic DRM. In order to further improve the efficiency of the photocatalytic DRM process, several strategies including doping with Cu, Pt and Ag, La and montmorillonite have been exploited to accelerate charge transfer and

promote the reactant conversion. Besides, narrow bandgap materials (such as black TiO_2 and graphitic carbon nitride) have also been developed to extend the range of light absorption.

Tahir and co-workers [75] reported that carbon dioxide was selectively reduced to carbon monoxide with the productivity of 237.5 $\mu mol \cdot g_{cat}^{-1} \cdot h^{-1}$ over montmorillonite (MMT) doped titanium oxide (MMT/TiO_2) in the presence of methane under UV irradiation at temperature of 100 °C. MMT/TiO_2 exhibited 2.52 times higher photoactivity than the bare TiO_2 counterpart. They suggested that the electron trapping in MMT reduced charge recombination and enhanced desorption of products, and MMT also contributed to the reactant adsorption. In another work [76], they further introduced nickel doping on MMT/TiO_2 and achieved carbon monoxide and hydrogen productivities of 750 and 1126 $\mu mol \cdot g_{cat}^{-1} \cdot h^{-1}$, respectively. They suggested that in addition to the promotion effect of MMT, nickel prevents charge recombination and provides more active sites for the reduction of carbon dioxide (**Figure 11**). Similarly, promotion with basic lanthanum oxide has attracted attention for enhancing the adsorption of carbon dioxide in photocatalytic DRM [77]. Tahir and co-workers [78] also investigated La doped TiO_2 for photocatalytic DRM under UV irradiation at mild conditions, and achieved carbon monoxide and ethane productivities of 425 and 246.4 $\mu mol \cdot g_{cat}^{-1} \cdot h^{-1}$, respectively. It was found that pure TiO_2 tended to produce carbon monoxide, while the La-doped sample was more selective to hydrocarbons. The enhanced photocatalytic performance was attributed to efficient reactant adsorption and promoted charge separation.

In addition to the wide bandgap photocatalyst, the narrow bandgap materials have been exploited to make photocatalytic DRM feasible under simulated light or visible solar light. Hu and co-workers [79] reported an efficient photocatalytic DRM over Pt/black TiO_2 under visible light at catalyst surface temperature of 550 °C, and achieved a hydrogen and carbon monoxide productivities of 71 $mmol \cdot g_{cat}^{-1} \cdot h^{-1}$ and 158 $mmol \cdot g_{cat}^{-1} \cdot h^{-1}$, respectively. It was

found that the enhanced yields under irradiation were due to the photocatalytic reaction. On the basis of FT-NIR and EPR characterization, they suggested that the oxygen vacancies of the black TiO_2 formed a donor level (Ti^{3+}) below the CB of TiO_2, thus an additional energy bandgap of 1.3 eV enabled the absorption of visible light. Moreover, Pt loading greatly accelerated the charge transfer and contributed to the C-H bond cleavage.

Tahir et al. [80] studied the La-doped graphitic carbon nitride (La/g-C_3N_4) for selective photocatalytic DRM under visible light at mild conditions and achieved carbon monoxide and hydrogen productivities of 602 $\mu mol \cdot g_{cat}^{-1} \cdot h^{-1}$ and 38.5 $\mu mol \cdot g_{cat}^{-1} \cdot h^{-1}$, respectively. Traces of C_2H_6 were also observed. The Cu-loaded graphitic carbon nitride nanorods (Cu/g-C_3N_4) were investigated for selective photocatalytic DRM under simulated solar irradiation at mild temperature and exhibited the carbon monoxide and hydrogen production rates of 142 $\mu mol \cdot g_{cat}^{-1} \cdot h^{-1}$ and 76 $\mu mol \cdot g_{cat}^{-1} \cdot h^{-1}$, respectively [81]. In another work, Liu and co-workers [82] reported that zinc doping effectively broadened the light absorption range of g-C_3N_4 with the bandgap of 2.54 eV. Zn-g-C_3N_4 selectively produced carbon monoxide and hydrogen with productivities of 666.75 $\mu mol \cdot g_{cat}^{-1} \cdot h^{-1}$ and 155.24 $\mu mol \cdot g_{cat}^{-1} \cdot h^{-1}$, respectively. Ruthenium was loaded as co-catalyst upon the Zn-g-C_3N_4 sample for the same process and selectively produced carbon monoxide, acetaldehyde and ethanol with the rates of 479.00 $\mu mol \cdot g_{cat}^{-1} \cdot h^{-1}$, 130.38 $\mu mol \cdot g_{cat}^{-1} \cdot h^{-1}$ and 500.45 $\mu mol \cdot g_{cat}^{-1} \cdot h^{-1}$, respectively. The Zn incorporation resulted in N-Zn bands that promoted the separation and transfer of charge carriers, and at the same time, provided more alkaline sites for the adsorption of carbon dioxide. Ru loading not only further accelerated the charge separation and promoted the charge transfer from g-C_3N_4 to Ru nanoparticles, but also enhanced the adsorption/desorption of the reactants/products, thus produced various chemicals. The charge transfer process and surface reaction mechanism of methane conversion over the Ru/Zn-g-C_3N_4 photocatalysts are shown in **Figure 12**.

In addition to noble metals such as platinum, Ni and Cu are potential plasmonic promoters for photocatalytic methane activation. Nickel has been widely studied in thermocatalytic methane conversion due to its high activity and lower price. Ye and co-workers [42,83] discovered that Ni effectively promoted DRM over Ni/Al_2O_3 and Ni/SiO_2 nanocomposites under light irradiation at 550 °C, in which Ni nanoparticles acted as both the catalytically active sites and a plasmonic promoter. Li and co-workers [84] reported a Ni/CeO_2 nanocomposite for light-driven DRM under focalized UV-vis-Infrared irradiation without any other heater, which achieved hydrogen and carbon monoxide productivities of 391.8 $\mu mol \cdot g_{cat}^{-1} \cdot h^{-1}$ and 376.2 $\mu mol \cdot g_{cat}^{-1} \cdot h^{-1}$, respectively, with the light to fuel efficiency of 11.1%. They suggested that LSPR on the Ni nanoparticles and significant IR heating effect causing the equilibrium temperature increase up to 807 °C on the nanocomposite, CeO_2 also played an important role for reactant activation and durability enhancement due to its intrinsic activity for DRM and carbon elimination ability by the abundant lattice oxygen. Nevertheless, their reaction conditions were still harsh, especially for necessary huge thermal energy input. Yoshida et al. [85] reported plasma-assisted DRM over Ni/Al_2O_3 under visible light irradiation at 200 °C, with carbon monoxide and hydrogen productivities of 1.87 and 1.20 $mmol \cdot h^{-1}$, respectively. Moreover, Ni/Al_2O_3 was inactive in the same thermal condition without light irradiation, thus metallic Ni nanoparticles were responsible for the photocatalytic DRM performance under visible light irradiation.

Ye and co-workers [44] reported for the first time that plasmonic promoter Au was effective in the activity enhancement of thermocatalytic DRM over Rh-Au/SBA-15 under low intensive visible light irradiation at 500 °C, with the hydrogen and carbon monoxide productivities of 3700.0 and 4050.0 $\mu mol \cdot g_{cat}^{-1} \cdot s^{-1}$, respectively. The productivities were higher than the sum of that of Au/SBA-15 and Rh/SBA-15 under the same conditions. The UV/VIS spectra showed that the Au containing samples exhibited visible light absorption

due to the Au LSPR, and the intensity of electromagnetic field around metal nanoparticles in Rh-Au/SBA-15 was much enhanced due to the near field coupling effect. High temperature increased the energy of the photoinduced hot electrons, while plasmonic metal nanoparticles contributed to the reactant polarization and the energetic hot electrons enhanced molecular activation. Afterwards, similarly, bimetallic alloy nanocomposites Pd-Au/Al_2O_3 [86] and Pt-Au/SiO_2 [87] all exhibited considerably enhanced catalytic performance in DRM under visible light irradiation at milder temperature largely due to the strong LSPR of plasmonic metal nanostructures.

Recently, Zhou and co-workers [88] fabricated a Cu-Ru single-atom alloy, which consisted of catalytic single-Ru atoms supported on Cu nanoparticles for DRM under laser without external heating and achieved a long-term stability for 50 hours with methane conversion of 220 $\mu mol \cdot g_{cat}^{-1} \cdot s^{-1}$ and selectivity of above 99%. They suggested that single-Ru atom active sites, together with the Cu nanoparticle LSPR, were responsible for the prominent photocatalytic performance, in which plasmonic Cu nanoparticles facilitated the generation of hot electrons, while the single-Ru atoms provided highly active sites for methane dehydrogenation and carbon dioxide activation as shown in **Figure 13a**. Moreover, a proper single-atom structure was essential. Calculations showed that the structure consisting of isolated Ru atoms on Cu surface was optimal for lowering molecular activation barriers and resisting other processes such as reverse water gas shift reaction and coke formation. Coke produced upon Ru ensembles and Cu surface blocked the active sites and caused the catalyst deactivation (**Figure 13b**). Note that the Cu-Ru single-atom alloy showed much higher activity and longer durability in photocatalytic DRM than in thermocatalytic DRM.

Note that semiconductors often contain crystallized and condensed water, which may strongly affect [89] the charge transport processes and activation energies. Both the additional and structural water would have important influences on the photocatalytic

methane reforming processes. This phenomenon should be taken into consideration in DRM. Zoltán Kónya [90] et al. investigated the roles of water on the significantly improved H_2 production rate over the Rh modified nanostructures in the photocatalytic CH_4-CO_2-H_2O system. They demonstrated that the dissolved CO_2 in carbonate acted as hole scavenge, hence elongated the lifetime of the electron-hole pair [91]. Additionally, the hydrogen carbonates trapped by a hole can also generate OH• radicals, which can be responsible for the increased activity. Moreover, they also confirmed the role of structural H_2O/-OH in photocatalysis.

2.2.2. Steam reforming of methane (SRM)

Yoshida et al. [92] discovered photocatalytic SRM over Pt/TiO_2 under UV irradiation at room temperature. Hydrogen and carbon dioxide were observed as main products with trace amounts of ethane and carbon monoxide. The isotopic experiments suggested that the interaction of methane and water firstly generated the [CH_2O] intermediates, which then further reacted with water and produced hydrogen and carbon dioxide. Similarly, they further investigated β-Ga_2O_3 and Pt/β-Ga_2O_3 in photocatalytic SRM using 300 W Xe lamp at mild temperature. Hydrogen and carbon dioxide were detected as products. An improved hydrogen productivities of 1 $\mu mol \cdot min^{-1}$ g^{-1} was obtained in the steady state over Pt/β-Ga_2O_3 [93]. Besides, $NaTaO_3$ with high photoactivity in the water decomposition was used for photocatalytic SRM using 300 W Xe lamp at mild temperature. Compared to bare $NaTaO_3$, enhanced photocatalytic SRM performances were observed over the samples modified either by Pt or La, while the Ni-loaded sample could not activate methane and just showed high photoactivity for the water decomposition [94,95]. Li et al. [96] reported an enhanced photocatalytic hydrogen evolution over Pt/TiO_2 under UV irradiation (wavelength centered at 254 nm) at mild temperature by integrating water splitting with methane conversion. The

hydrogen productivity of 200 μmol·g_{cat}^{-1}·h^{-1} was achieved, ethane and carbon dioxide were simultaneously produced with the rates of 53.3 μmol·g_{cat}^{-1}·h^{-1} and 28.9 μmol·g_{cat}^{-1}·h^{-1}, respectively. Pt sites seem to play an important role in the methane activation, and ethane comes from the coupling of methyl radicals.

In another work, Yoshida et al. [97] reported that compared to bare $K_2Ti_6O_{13}$, Pt loaded $K_2Ti_6O_{13}$ showed significantly enhanced photocatalytic SRM performance in the same conditions using a 300 W Xe lamp at mild temperature, and Rh loaded $K_2Ti_6O_{13}$ exhibited two times higher activity than Pt loaded $K_2Ti_6O_{13}$. It was found that not only the type of loaded metal but also the loading method influenced the photocatalytic SRM performance. They suggested that metallic rhodium nanoparticles and rhodium oxide nanoparticles coexisted in Rh loaded $K_2Ti_6O_{13}$ and promoted the transfer and separation of charge carriers. The proposed mechanism and band structures are shown in **Figure 14**, the photogenerated holes and electrons are transferred to rhodium oxide nanoparticles and metallic rhodium nanoparticles, respectively. This could efficiently prevent the charge recombination and cooperatively promoted the reduction and oxidation processes.

Amin et al. [98] discovered a photocatalytic bi-reforming of methane (BRM) process combined by photocatalytic DRM and SRM over Ag loaded protonated graphitic carbon nitride (Ag/pg-C_3N_4) under UV irradiation (wavelength centered at 254 nm) at mild conditions. It was found that carbon monoxide, hydrogen and methanol were the main products, in addition to traces of ethane in all the photocatalytic SRM, DRM and BRM processes. Interestingly, pure g-C_3N_4 was favorable for CO evolution, while pg-C_3N_4 promoted both H_2 and CH_3OH production. Compared to the photocatalytic SRM and DRM processes, in photocatalytic BRM, the production of methanol almost remained unchanged with the rate of 365 μmol·g_{cat}^{-1}·h^{-1}, while that of carbon monoxide and hydrogen increased to 1211 μmol·g_{cat}^{-1}·h^{-1} and 344 μmol·g_{cat}^{-1}·h^{-1}, respectively (**Table 1**). Ag loading and

protonation of g-C_3N_4 promoted charge separation and thus improved reactant adsorption. The proposed mechanism of methane conversion over Ag/pg-C_3N_4 is shown in **Figure 15**.

2.3. Photocatalytic coupling of methane

Methane coupling could be an efficient way to selectively convert methane into higher hydrocarbons, such as ethane and propane. Methane coupling includes the non-oxidative coupling of methane (NOCM) and oxidative coupling of methane (OCM). In addition to hydrocarbons, OCM can also produce carbon monoxide and carbon dioxide as by-products.

NOCM: $2CH_4 \rightarrow C_2H_6 + H_2$ (8)

OCM: $4CH_4 + O_2 \rightarrow 2C_2H_6 + 2H_2O$ (9)

$2CH_4 + O_2 \rightarrow C_2H_4 + 2H_2O$ (10)

The production of ethylene (Eq. 10) does not usually occur in the photochemical coupling. Ethane seems, to be one of the primary products of the photocatalytic coupling. Ethane dehydrogenation to ethylene is thermodynamically unfavorable at ambient temperature and does not seem to be catalyzed by photocatalysts.

The photoinduced centers of some metal oxides, such as of Zn, Ti, Al and Ga oxides, are capable to dissociate methane under mild conditions with the role of photogenerated O^- holes. Among them, TiO_2 was studied in methane coupling and showed predominant CO_x production and low methane conversion in both OCM and NOCM [99,100].

Ga_2O_3 has been investigated as a promising material in NOCM under UV irradiation at mild temperature and exhibited much higher methane conversion and higher ethane selectivity (up to 96%) than other oxide semiconductors, with high stability in the reductive atmosphere [74,101]. Silica materials were also exhibiting NOCM activity after high temperature pretreatment, which generated $\equiv Si - O\bullet$ as photoactive sites via the dehydroxylation of surface hydroxyl groups [102]. More often, promotion with metals could further improve the

photocatalytic NOCM performance by enhancing charge separation, accelerating charge transfer and acting as a co-catalyst.

Highly dispersed mixed metal oxide species, such as SiO_2-Al_2O_3-TiO_2, ZrO_2/SiO_2, MgO/SiO_2 Ce/Al_2O_3 and $Ce/Ti/SiO_2$ have been investigated in NOCM at mild conditions. They exhibited higher photoactivity and ethane selectivity of above 90% [26,101,103,104]. These highly dispersed metal oxide species showed different electronic and local structures from the original bulk materials [101,105]. Among them, the SiO_2-Al_2O_3-TiO_2 ternary oxide has been reported as one of the most effective photocatalysts for NOCM with the methane conversion rate of around 1.40 $\mu mol \cdot g_{cat}^{-1} \cdot h^{-1}$, corresponding to the ethane productivity of 0.69 $\mu mol \cdot g_{cat}^{-1} \cdot h^{-1}$. However, the total C_{2+} yield of 3.74% was still very low even after 90 h of reaction [103].

Chen et al [106]. investigated a zinc modified medium pore ZSM-5 zeolite photocatalysts, which achieved prominent photocatalytic NOCM performance under UV irradiation at room temperature. The methane conversion of 23.8% was achieved in 8 h and ethane selectivity was above 99.0%, corresponding to the ethane production rate of 5.95 $\mu mol \cdot g_{cat}^{-1} \cdot h^{-1}$. Note that the photocatalyst operated without obvious deactivation and coke deposition for 16 h. They suggested that the existence of univalent zinc species (Zn^+) played a key role in the efficient methane activation through the photoinduced electron attack from Zn 4s orbital to the empty C-H σ^*-antibonding orbital (**Figure 16b**). Besides, the pores with an approximate size of 0.55 nm restricted the formation of longer chain C_{3+} hydrocarbons. Thus, a higher selectivity towards ethane was achieved. A two-stage photocatalytic process was proposed, in which UV and visible light accomplished the charge transfer from oxygen of the zeolite framework to Zn^{2+} and the methane activation upon the Zn^+ species (**Figure 16a**). Consequently, the photocatalyst still exhibited outstanding performance under sunlight irradiation, with the methane conversion of 0.63 $\mu mol \cdot g_{cat}^{-1} \cdot h^{-1}$ and ethane selectively above

99.9%. The activity of the photocatalyst decreased in the presence of water, which limited its application in the water-based photocatalytic systems.

Li et al. [48] further investigated the Ga^{3+} modified ETS-10 titanosilicate in photocatalytic NOCM under UV irradiation at mild temperature and achieved methane conversion rate of 29.8 $\mu mol \cdot g_{cat}^{-1} \cdot h^{-1}$ without the CO_x formation, corresponding to the methane conversion of 14.9% and ethane selectivity higher than 70%. Furthermore, the Ga^{3+} modified sample could be regenerated after thermal treatment in moist air without noticeable deactivation for 5 cycles. It revealed that only after the ion-exchange of ETS-10 with the particular metal ions such as Ga^{3+}, Al^{3+}, Zn^{2+} and Fe^{3+}, the enhanced photocatalytic activity could be observed. Among them, the Ga^{3+} modified sample showed the best performance, the Al^{3+}, Zn^{2+} and Fe^{3+} modified samples were inferior, while the Cu^{2+} modified sample was inactive. They suggested that the ion-exchange treatment formed the structure defects in the framework of ETS-10 and thus, resulted in the abundant Ti-OH groups. Besides, the modified metal cations played an important role in polarizing methane and thus reduced the activation energy for C-H cleavage. The proposed mechanism over Ga^{3+} modified ETS-10 is shown in **Figure 17**. The photoexcitation firstly occurs upon the titanate composite in ETS-10. The Ti-OH groups then trap the photogenerated holes to generate active hydroxyl radicals for the H abstraction. The Ti-OH groups could be then regenerated in the presence of water and oxygen under high temperature.

In another work, Zhang and co-workers [36] fabricated a Pt loaded hierarchical macro-mesoporous structure (HGTS) consisting of Ga dopant and porous TiO_2-SiO_2 for photocatalytic NOCM using a 300 W Xe lamp under mild temperature. The methane conversion of 6.24% was achieved in 4 h, corresponding to the methane conversion rate of 3.48 $\mu mol \cdot g_{cat}^{-1} \cdot h^{-1}$ and 90% selectivity toward ethane. It was found that the optimized Ga doping was beneficial for promoting charge separation, while doping with Pt further

significantly accelerated charge transfer from TiO_2 to the Pt sites due to the Mott–Schottky junction between Pt and TiO_2. Interestingly, Ga substitution in the framework reduced the electron transfer from surface oxygen vacancy to the Pt site. Methane was more easily activated by the electron-enriched metallic Pt, while the cationic Pt helped to abstract H atoms. However, the photocatalytic activity decreased by almost a half after four cycles.

Combining of semiconductor and plasmonic nanostructures can also contribute to the enhancement of methane coupling. Long et al. [107] reported Au/ZnO nanocomposite consisting of plasmonic Au nanoparticles and ZnO nanosheets with polar 001 plane in light-driven NOCM process under simulated solar light irradiation at room temperature. The optimized Au/ZnO (001) nanocomposite exhibited ethane and hydrogen productivities of 11.0 $\mu mol \cdot g_{cat}^{-1} \cdot h^{-1}$ and 10.0 $\mu mol \cdot g_{cat}^{-1} \cdot h^{-1}$, respectively. They suggested that the coupling of the intrinsic inner electric field (IEF) of ZnO nanosheets and LSPR field of Au nanoparticles significantly accelerated the charge separation in photoexcited ZnO and promoted the electron transfer to Au nanoparticles. This makes the ZnO surface more electron poor and favored methane chemisorption and dissociation (**Figure 18 a**). The proposed mechanism was shown in **Figure 18 b**. Methane was firstly polarized in the ZnO surface and then oxidized by the holes to form $Zn\text{-}CH_3\bullet$ and H^+ species. Ethane was finally produced by the coupling of two methyl radicals, while the electrons were injected into the molecular orbitals of H^+ to generated hydrogen. A similar strategy was effective for methane coupling over Au/TiO_2 (001).

The presence of CO_2 in the reaction mixture can also enhance the methane coupling with ethylene being the major product. Recently, Liu and co-workers reported that methane and carbon dioxide were selectively converted into ethylene and carbon monoxide over the plasmonic Ag loaded TiO_2 nanocomposite under simulated solar irradiation at room temperature, with the ethylene and carbon monoxide productivities of 686.0 $\mu mol \cdot g_{cat}^{-1} \cdot h^{-1}$

and 1149.0 μmol·g_{cat}^{-1}·h^{-1}, respectively [108]. It was found that both the visible light and UV light were critical for the enhanced photocatalytic performance (**Figure 19 f**). Visible light aroused the LSPR over Ag nanoparticles, while UV light excited the photoelectric effect on TiO_2 (**Figure 19a**, **c and e**). As a result of the balanced electron transfer between Ag and TiO_2, the photoinduced hot electrons over plasmonic Ag were rapidly injected into the adjacent TiO_2 (**Figure 19d**), leading to the abundant formation of Ag(I) or hot holes. The holes on TiO_2 were rapidly consumed by the hot electrons from Ag, resulting in a high density of electrons on TiO_2, which promoted the chemisorption and reduction of carbon dioxide toward carbon monoxide. In a word, the synergy of the visible light induced LSPR effect over Ag nanoparticles and UV light induced photoelectric effect on TiO_2 achieved the enhanced photocatalytic performance under simulated solar irradiation. The special interfacial states between loaded metals and supports were suggested to be important for photocatalytic performance, such as active sites and Schottky barrier (**Figure 19 g, h**). The optimized CuPt mixed catalyst supported over TiO_2 showed [109] high activity in the methane coupling in a flow reactor with the selectivity to the C_2 products of 60%. The copper species play the role of cocatalyst, while Pt has shown the plasmonic effect, which slows down the charge carrier recombination.

Recently, our group proposed [110] photochemical looping for methane coupling at room temperature over the silver-heteropolyacid-titania nanocomposites (Ag-HPW/TiO_2). We suggested that the n-type semiconductor TiO_2 and the p-type semiconductor HPW created a p-n heterojunction between their interface. Under the irradiation, photogenerated electrons were rapidly transferred from TiO_2 to HPW and resulted in silver reduction, while the abundant photogenerated holes were accumulated in TiO_2 and enhanced methane oxidation. The coupling reaction involves two methyl radicals produced via methane activation over silver sites. The reaction slowed down with the reduction of silver cations. Promisingly, the

nanocomposite can be reversibly regenerated by exposing it to air under irradiation at room temperature, after which the nanocomposite still exhibited the original performance for methane coupling in numerous cycles (**Figure 20a**). The amount of the produced ethane exactly corresponds to the silver content in the nanocomposite. The photochemical looping process achieves methane coupling selectivity over 90%, quantitative yield of ethane over 9%, high quantum efficiency (3.5% at 362 nm) and excellent stability. (**Figure 20b**).

3. Major routes of methane photocatalytic conversion: challenges and outlook

A sharp increase in the interest to the methane photocatalytic conversion has been observed in the last decade (**Figure 5**). Three major routes of methane photocatalytic conversion have attracted particular attention. They involve

- methane selective oxidation with the methanol being the principal reaction product;
- methane photocatalytic dry or steam reforming to hydrogen and carbon monoxide;
- methane coupling leading to the formation of ethane and higher hydrocarbons.

The semiconductors, co-catalysts and products obtained in these three major methane photocatalytic conversion routes are displayed in **Figure 21**. Much less information is available about other methane conversion reactions. A recent paper by Hu [111] et al reports the possible use of methane and other light alkanes in the amination, alkylation, and arylation reaction over ceria photocatalysts. Direct methane aromatization with simultaneous hydrogen production was recently uncovered [112] over Si-doped GaN nanowires under ultraviolet illumination at ambient temperature.

Let us discuss the advantages and drawbacks of each methane conversion route. Methane photocatalytic oxidation may lead to methanol, formaldehyde, formic acid, CO and CO_2. Extremely low yields of formaldehyde and formic acid were reported in the methane

photocatalytic conversion. Among different oxidation processes, methane partial oxidation to methanol and methane complete oxidation to CO_2 have attracted particular attention. The complete oxidation of methane to CO_2 seems to be an attractive option to reduce the concentrations of methane present in the atmosphere. Note that methane is a GHG, which is 30 times more potent than carbon dioxide. Methane photocatalytic oxidation is an exothermic process. The methane photocatalytic oxidation to CO_2 can reduce, on the one hand, global warming and on other hand, because of the exothermic effect, it can produce renewable electricity under mild conditions.

Methanol is the target product in most of the publications dedicated to methane photocatalytic oxidation. The photocatalytic oxidation to methanol requires oxidizing agents, such as molecular oxygen, hydrogen peroxide, water or NO. The use of different oxidizing agents leads to different methanol productivities. Important, methane oxidation with water or hydrogen peroxide results in several times higher productivities compared to the methane oxidation in the presence of molecular oxygen. Since the methane photocatalytic oxidation commonly proceeds with the radical mechanisms, the reasons of a higher rate of methane conversion in the presence of water or hydrogen peroxide can be due to the much easier generation of oxygen or hydroxyl radicals for the methane activation. The selectivity of methane conversion to a larger extent depends on the concentration and reactivity of the generated radical species. Among the methane oxidizing agents, water seems to be the most efficient. It enables at the same time, the highest methane conversion rate and high selectivity to methanol. A much higher cost of hydrogen peroxide compared to methane and methanol hinders its utilization for methane photocatalytic conversion. The reactive oxygen for methane photocatalytic oxidation can be also provided by the semiconductor or cocatalysts. In this case, the reaction proceeds according to the Mars-van Krevelen mechanism [30] with periodic

reduction and re-oxidation of photocatalysts. This mechanism was clearly identified over silver [54] and zinc [30] catalysts.

The literature shows a major progress in productivity of methane to methanol conversion (**Figure 22a**). Thus, from 2005 to 2020 the productivity for the best catalysts known so far increased from 529 to 2556 μmol g^{-1} h^{-1}. The highest efficiency has been observed over oxides like WO_3, TiO_2, NiO, Ag/WO_3 and Au supported over ZnO.

Methane photocatalytic reforming usually leads to hydrogen and carbon monoxide. Direct synthesis of oxygenates from methane and carbon dioxide currently seems to be highly challenging, though production of small amounts of acetone was reported by Shi [73] et al. over the $Cu/CdS–TiO_2/SiO_2$ catalyst under ultraviolet irradiation. The characteristic productivities for methane photocatalytic reforming are much higher than for methane oxidation to methanol. The methane dry photocatalytic reforming has been investigated in greater detail compared to the steam reforming process. Very often, the photocatalytic reforming proceeds at elevated temperatures (>100°C and even >550°C), when a contribution of thermal activation to the methane conversion rate cannot be excluded. Important, the composition of syngas produced via methane dry photocatalytic reforming is different from that, which could be expected from the stoichiometric reaction: $H_2/CO=1$; $CH_4+CO_2 \rightarrow H_2+CO$. This suggests a possible contribution of water gas shift and other processes to the methane photocatalytic reforming. Methane photocatalytic reforming to syngas can also simultaneously involve CO_2 and structural water of photocatalyst [90]. Methane photocatalytic reforming coincides with other methane reactions such as methane partial oxidation to methanol or methane coupling. That is also the reason, why the selectivity to carbon monoxide and hydrogen in methane photocatalytic reforming is rarely higher than 60-70%. The relatively rapid increase in the productivity of methane photocatalytic reforming has been observed recently (**Figure 22 b**). Thus, for the several last years, the productivity

increased almost ten times from 142 to 1211 μmol g^{-1} h^{-1}. The highest efficiency has been observed over silver supported nanoporous graphitic carbon nitride sheets.

Photocatalytic coupling to ethane and higher hydrocarbons represents an interesting path to upgrade methane. Indeed, ethane has a higher value than methane. Moreover, ethane can be converted via cracking/dehydrogenation to ethylene, which is an important platform molecule for many chemical processes. Different to the widely studied process of high temperature methane oxidative or non-oxidative [113] couplings (OCM and NOCM), methane photochemical coupling proceeds at lower temperatures. Low temperature photocatalytic coupling of methane produces mainly ethane, while ethylene, the building block of many daily basis plastic products, is commonly produced in high temperature methane oxidative coupling [3]. Both thermally activated and photoactivated methane coupling reactions proceed via the generation of CH_3 radicals. The primary product in both coupling processes is ethane. Note that in the higher temperature process, ethane is dehydrogenated to ethylene. At high temperatures, the ethylene formation from ethane is favored by thermodynamics. In contrast, ethane is primarily produced in the low temperature photocatalytic methane coupling. At low temperatures, dehydrogenation of ethane to ethylene is thermodynamically unfavorable and does not seem to be enhanced by photocatalysis.

Relatively high selectivity to ethane (often >70% and sometimes >90%) in the photochemical and photocatalytic methane coupling has been reported in many works. A trace amount of propane and even butane are often observed. The presence of propane and higher hydrocarbons arises from the coupling reaction of methane with ethane and other produced hydrocarbons. Despite better selectivity, the main challenge of methane photocatalytic coupling seems to be lower productivity compared to the methane partial oxidation or reforming. Recently, we suggested a new concept of photochemical looping for stoichiometric

synthesis of ethane from methane on the silver-based nanocomposites containing titania and heteropolyacids. The ethane productivity attained 20 μmol g^{-1} h^{-1} in this process.

The photocatalytic coupling of methane to ethane demonstrates significantly lower productivities in comparison with the methane oxidation to methanol or methane reforming. However, a gradual increase in the ethane productivity of ethane with time has been observed (**Figure 22 c**). Supported Ag, Zn and Ga based materials demonstrate productivities of ethane in the range 5 to 20 μmol g^{-1} h^{-1}.

The characteristic state-of the art productivities and selectivities of the major routes of methane photocatalytic conversion are summarized in **Table 2**. In terms of productivity, the three routes of methane photochemical conversion can be ranked in the following order: methane reforming> methane partial oxidation > methane coupling. The productivity ranges from >1000-2000 μmol g^{-1} h^{-1} in methane reforming or methane oxidation to methanol to 20 μmol g^{-1} h^{-1} in methane coupling. The opposite trend is observed for the selectivity of methane photocatalytic conversion processes. Higher selectivity is observed (**Table 2**) in the methane coupling to ethane followed by methane partial oxidation and then by methane reforming. Almost stoichiometric conversion of methane to ethane can be achieved in the photocatalytic process, while the selectivity of methane reforming is usually about 60-70%. Note that, because of the extremely low activity of photocatalysts in the methane conversion, the productivity data and in particular selectivity data might be not enough accurate. Some of the reaction products can be present in amounts beyond the detection limit of analyzing equipment (mass spectrometry, gas chromatography etc). In addition, some of the products can be adsorbed on the surface of photocatalysts and on the walls of photoreactors and thus, can become unavailable for analysis. Isotope tracing experiments can provide additional information about the methane photocatalytic conversion mechanism and about the origin of the reaction products.

Another important issue can be accurate control and determination of temperature in photocatalytic experiments. Exposure of the reacting system to a powerful lamp may result in a significant increase in the surface temperature in particular for the metals with plasmonic effect [45–47]. However, in numerous reports, the environmental temperature of the bed or water bath is considered as the real reaction temperature. Even temperature determination using a thermocouple in close contact with the catalyst can only be found in a limited number of works, which still could not be accurate enough due to the inevitable interference of irradiation and limited area of measurement. The development of more accurate and reliable temperature measurement methods has thus been a challenge that needs to be further addressed. For example, using of IR thermal cameras or in-situ micro-thermocouples (in contact with the catalyst surface) could be better alternatives.

Higher selectivity and productivity seem to be major challenges for the photocatalytic methane conversion. The photo-conversion efficiencies of photochemical methane conversions are generally lower than 10%. Higher solar-to-fuel efficiency of 12.5% has been reported [114] for DRM and that of 11.7% for photocatalytic oxidation of methane to methanol [115]. The photo-conversion efficiencies have been however generally lower than 5% or even 1% for photochemical methane coupling [107,110].

The separation of methane and products of methane photocatalytic conversion can be only feasible for practical purposes if the yield of target products can reach a few per cent. Another challenge is the stability of photocatalysts, though it has been rarely addressed in most of publications.

The efficiency of methane photochemical conversion can be improved by the design of new highly efficient photocatalysts, new photoreactors and processes. Engineering the band structure in the semiconductors, slowing down the charge carrier recombination and elaboration of efficient cocatalysts are principal ways for the optimization of the

photocatalytic performance in methane photocatalytic conversion. Control of band gap semiconductors have been applied to harness broader light range even visible light. Heterojunctions with semiconductors, metals and carbon-based materials have also been proven to be effective for charge carrier separation and recombination retardation. Adjusting band structure and redox potentials of methane reactions and corresponding reduction processes has been demonstrated [116] to be critical for completing photocatalytic cycles. The co-catalyst properties are particularly important for controlling the reaction selectivities. Polar nanostructures and plasmon resonance have been used to polarize and activate methane as well as to promote charge carrier separation [23,107]. The morphologies and structures of materials could have a significant influence on photocatalytic performance. The unique exposed facets or edges of the certain shapes of nanostructure make differences on surface reactions, which originate from the exposed surface area, charge carrier mobilities, sorption and other properties [63,117]. Highly efficient materials combining all the merits are expecting to be explored for photochemical methane conversions.

Currently, the majorities of photocatalytic methane conversion reactions are carried out in home-made or commercial batch reactors with various volumes. Relatively high residence time in batch reactors leads to the overoxidation of the methane conversion intermediates. Design of new photoreactors such as fluidized, slurry, fixed bed, membrane, optical-fiber, monolith or internally illuminated monolith photoreactors [118–121] can also enhance the efficiency of light collection, exposure of the photocatalyst to the irradiation, heat and mass transfer. Particular attention should be paid to the absence of even very tiny leaks. Even a very small amount of excess oxygen can affect the reaction rate and selectivity.

Further improvement in the selectivity of methane conversion can be achieved by the photochemical looping concept [110], which involves methane reaction over the solid materials followed by the solid carrier regeneration. The control of generation of oxygen and

hydroxyl radicals, methane and intermediates concentrations are major advantages of the photochemical looping concept leading to higher selectivity to the target products.

The current scientific immaturity of the methane photochemical conversion processes does not allow to envision industrial or practical utilization in the near future. Among the discussed methane photocatalytic conversion routes, the most promising could be photocatalytic methane oxidation to methanol. Methanol is a valuable platform molecule, it has a much higher cost compared to ethane produced by methane coupling or to syngas, which is manufactured by methane reforming. The methane partial oxidation to methanol exhibits relatively higher productivity and selectivity.

Electrocatalysis is also a promising strategy[17,122–124] for methane conversion to valuable produces. High temperature (T>500°C) methane electrocatalytic conversion usually results in syngas and ethylene, while at lower temperatures, methanol is obtained as a target product, though the kinetics of direct methane electrochemical conversion under mild conditions is extremely slow. The selectivity and activity of electrocatalysts can be adjusted and controlled by the voltage. Photoelectrocatalysis is similar to electrocatalysis with regard to the experimental setup and combines the advantages of both methods. Photoelectrocatalysis typically exploits semiconductor electrodes instead of normal conducting electrodes in electrocatalysis. Since solar energy is introduced into the system, photoelectrocatalytic conversion of methane would reduce electricity consumption. The sustainable electricity from solar energy or wind power can further improve the technology sustainability.

Direct mild conversion of methane is one of the main targets in the modern society. The photochemical processes such as methane partial oxidation, methane reforming and methane coupling should provide opportunities to perform methane conversion to value-added products, under mild conditions, instead of methane combustion. This should significantly

decrease the GHG effects due to the uncontrollable emission of methane and carbon dioxide and will contribute to the optimized utilization of fossil and renewable methane feedstocks.

Acknowledgement

This research is being performed within the ANR SolarMethaChem project (ANR-20-SODR-0002). The authors gratefully acknowledge the support of the French National Research Agency. D.H. thanks the China Scholarship Council for provide him a PhD stipend.

Credit author statement

Di Hu : Data Collection, Writing - Original Draft *Vitaly V. Ordomsky*: Conceptualization, Analysis, Review, Editing *A.Y. Khodakov* : Conceptualization, Writing, Review, Editing

Table 1. Yields of ethane, methanol, carbon monoxide and hydrogen in various photocatalytic processes over Ag/pg-C_3N_4 (CH_4/CO_2 =1.0, Temp=100 °C, from Ref. [98])

Feed gas	Process	Yields ($\mu mol \cdot g_{cat}^{-1} \cdot h^{-1}$)			
		C_2H_6	CH_3OH	CO	H_2
CH_4-H_2O	SRM	8	336	615	263
CO_2-CH_4	DRM	9	305	780	253
CH_4-CO_2-H_2O	BRM	7	365	1211	344

Table 2. Selectivity and productivity of different methane photocatalytic conversion routes

	Selectivity to the target products, %	Productivity, μmol·g_{cat}^{-1}·h^{-1}
Photocatalytic methane oxidation -to methanol -to carbon monoxide	 >40 >80	 5-20 (in air) and 2500 (in H_2O/O_2 or H_2O_2) 430 (in air)
Photocatalytic methane reforming DRM	 >60-70	 for H_2/CO >600-1200
Photocatalytic coupling of methane	>70-90	10-20

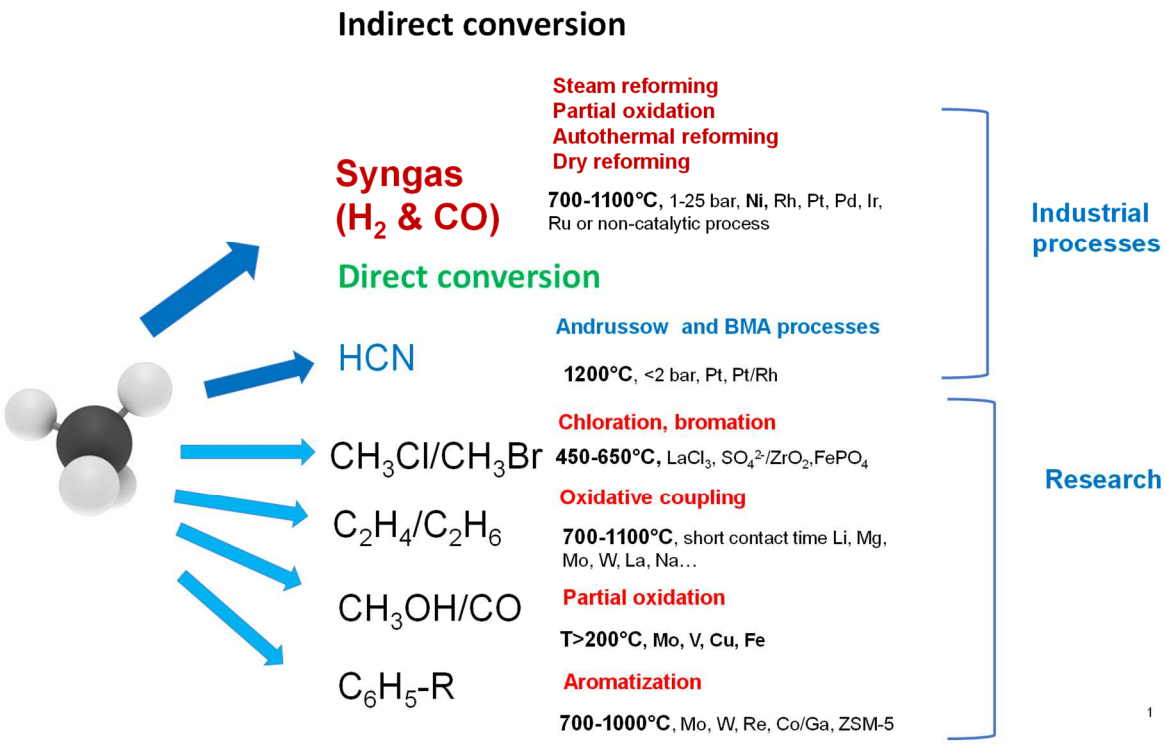

Figure 1. The state of the art direct and indirect methane chemical conversion. All the processes require high temperatures

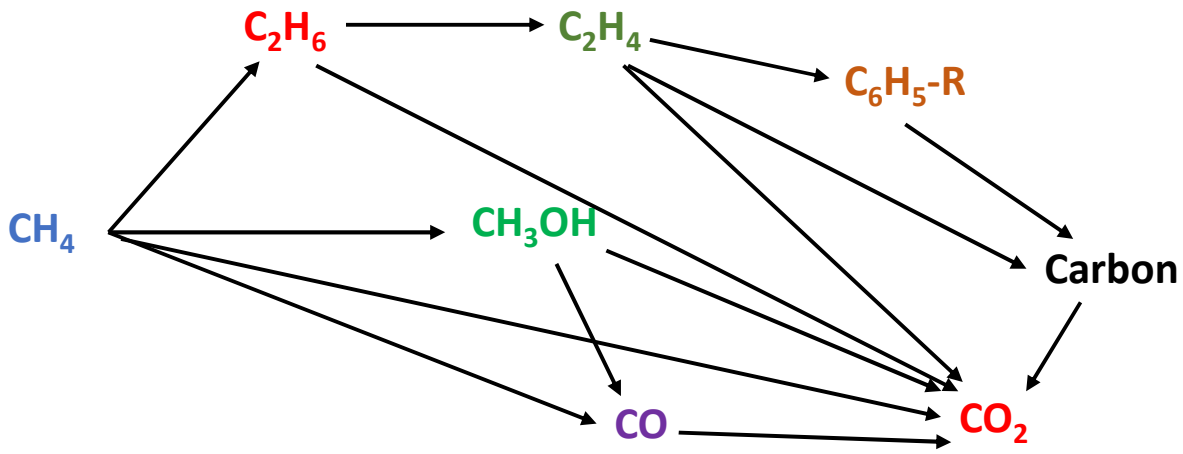

Figure 2. Most common reaction paths in methane conversion

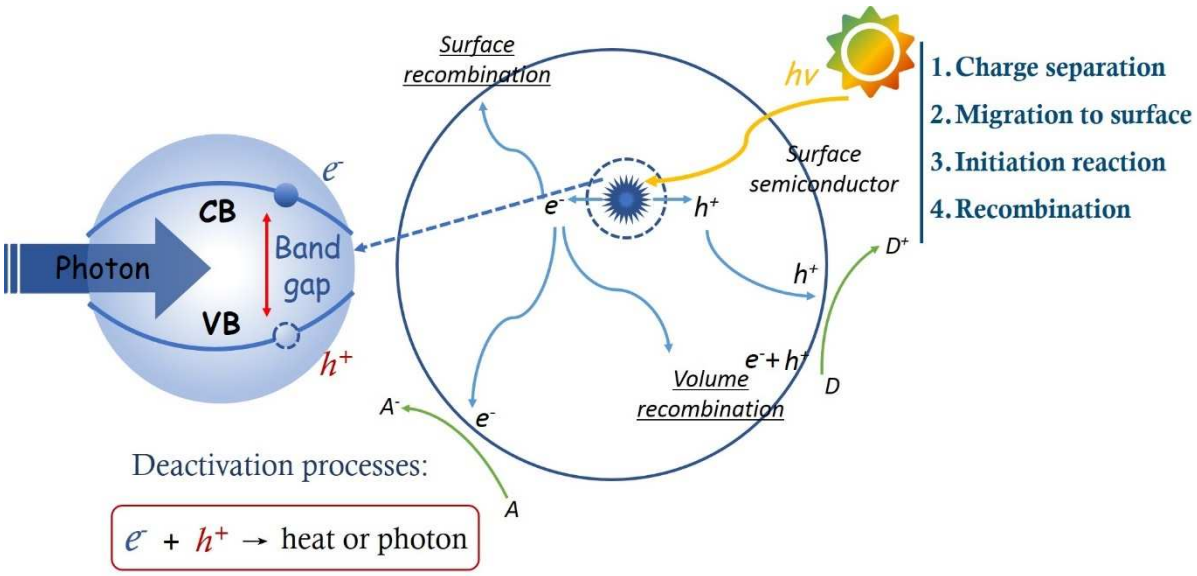

Figure 3. Photocatalytic excitation processes over semiconductors

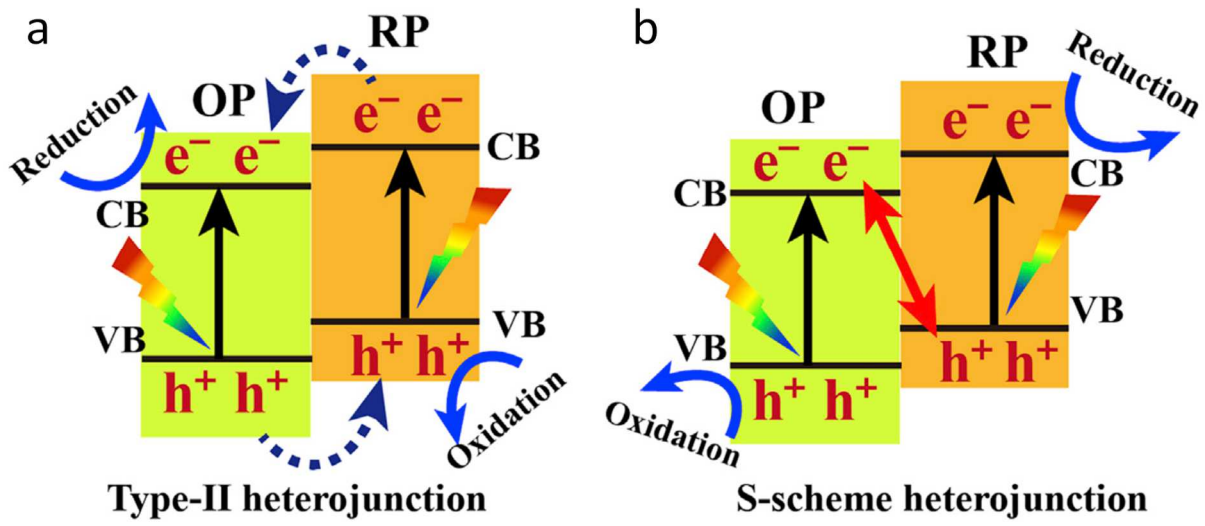

Figure 4. Band structure configuration and charge-transfer route of (B) type-II heterojunction and (C) S-scheme heterojunction (from ref. [33]).

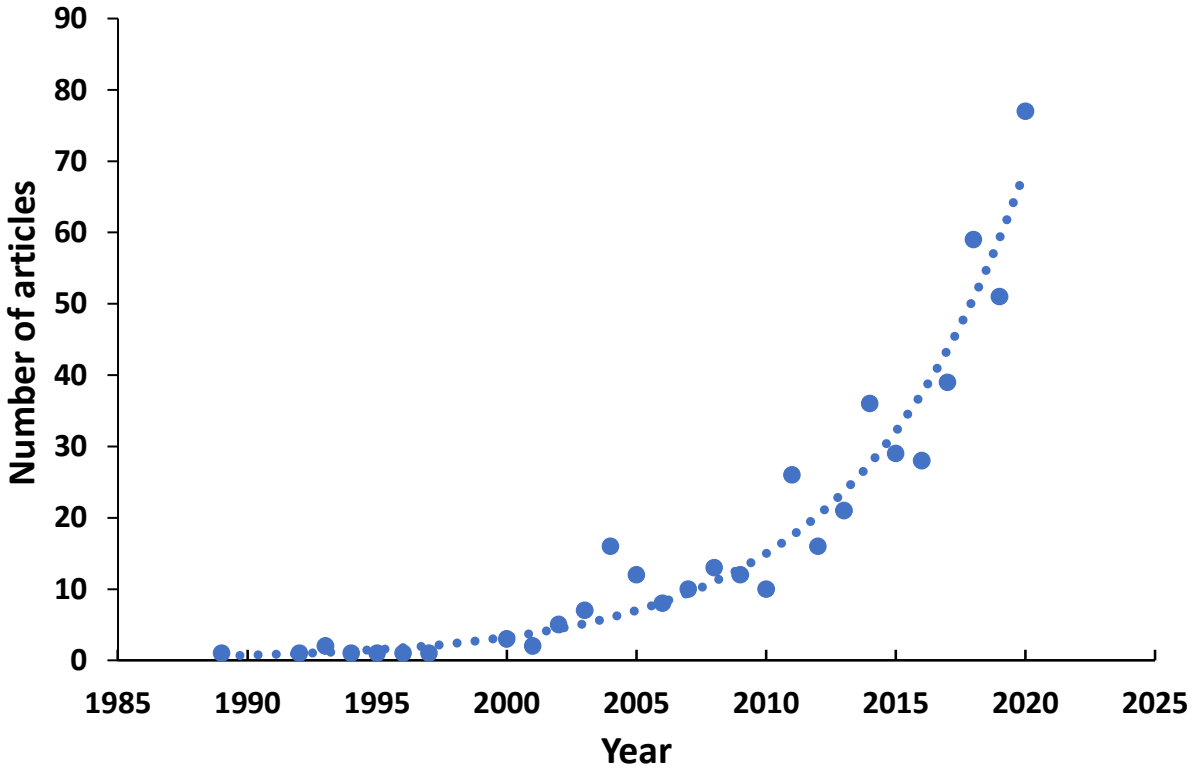

Figure 5. Evolution of the number of publications dedicated to methane photocatalytic conversion. Search results in Scopus using "methane" and "photocatalysis" as search items (December 31st, 2020).

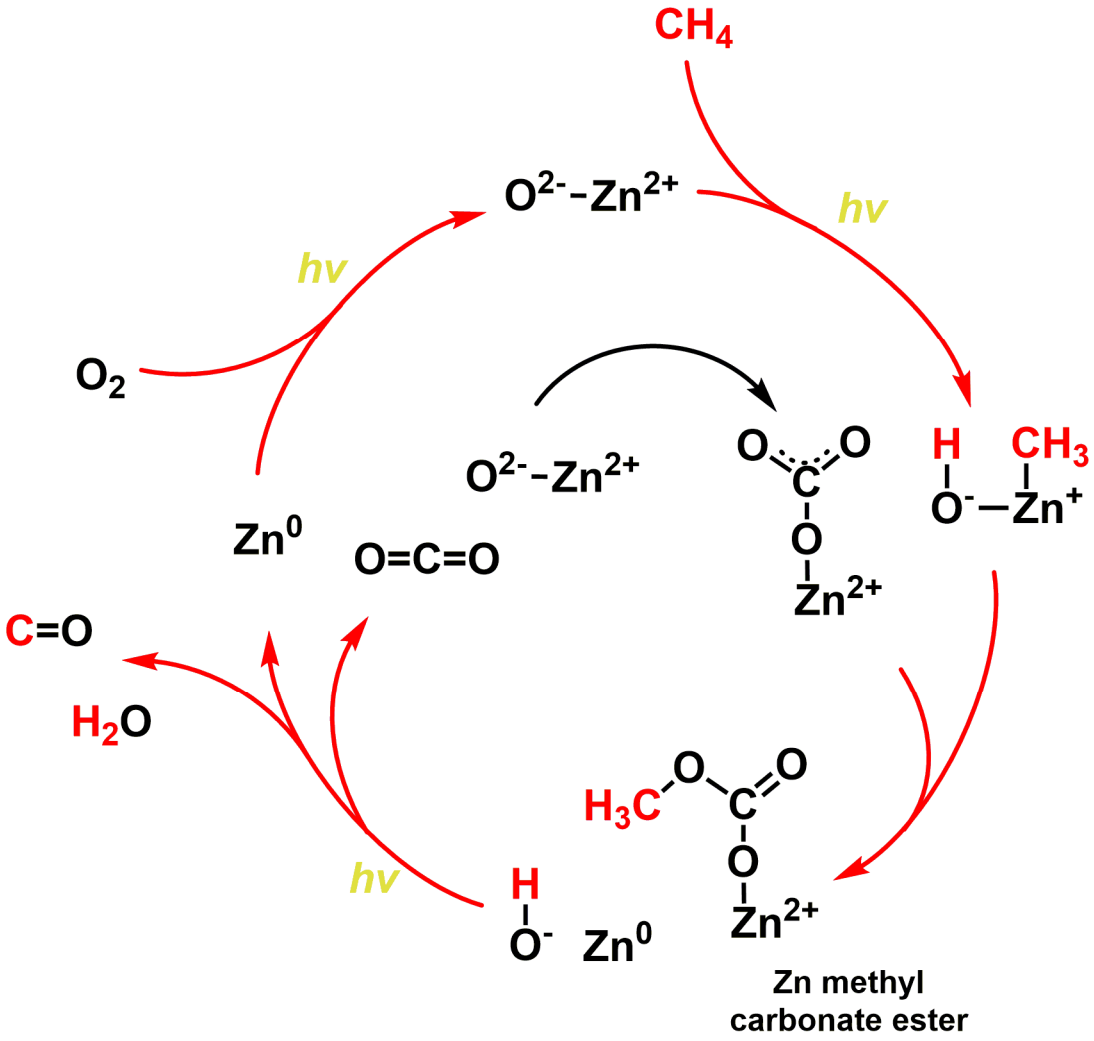

Figure 6. Reaction steps in methane oxidation with O_2 over Zn-HPW/TiO_2 (from Ref. [30])

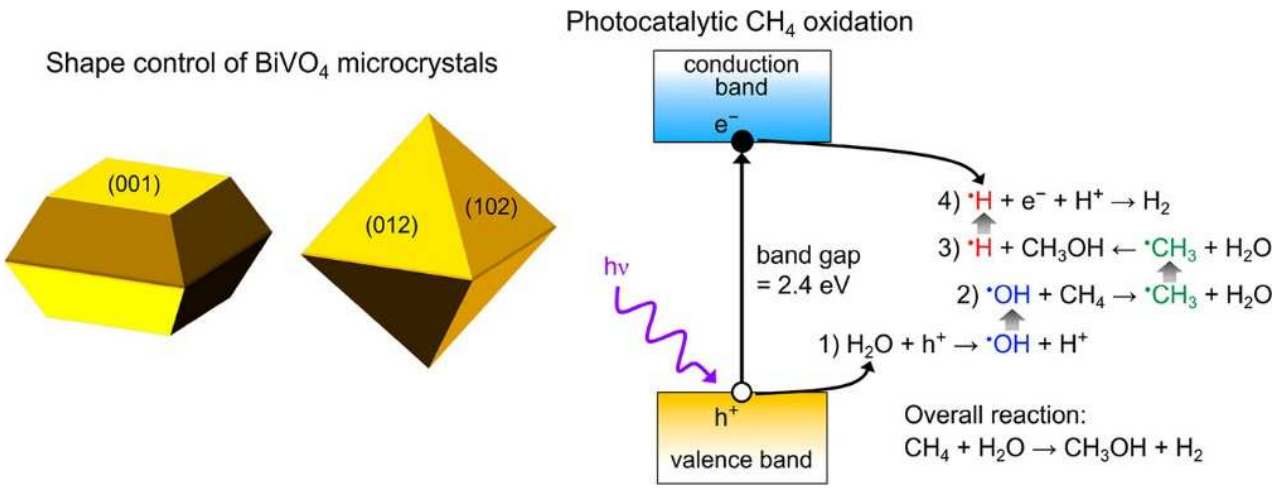

Figure 7. Catalyst structures and proposed mechanism of methane oxidation (from Ref. [63])

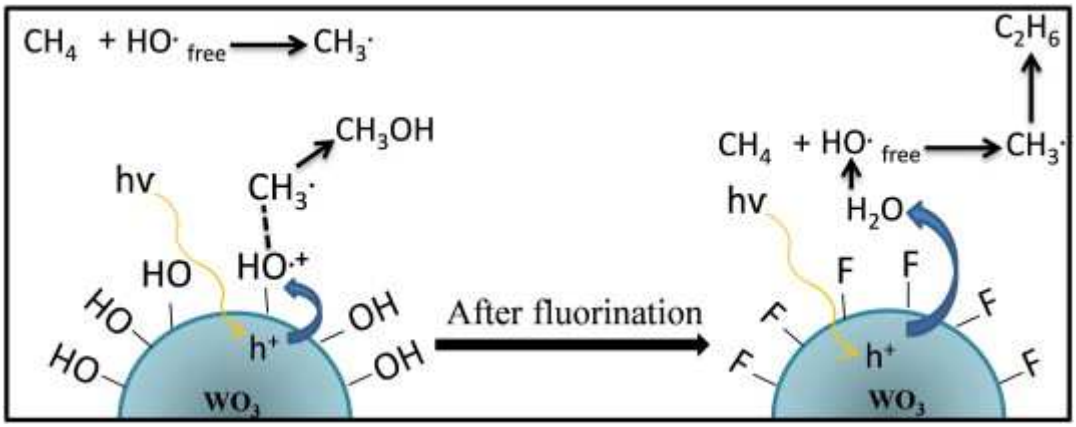

Figure 8. Proposed mechanism of methane oxidation over WO_3 before and after fluorination modification (from Ref. [66])

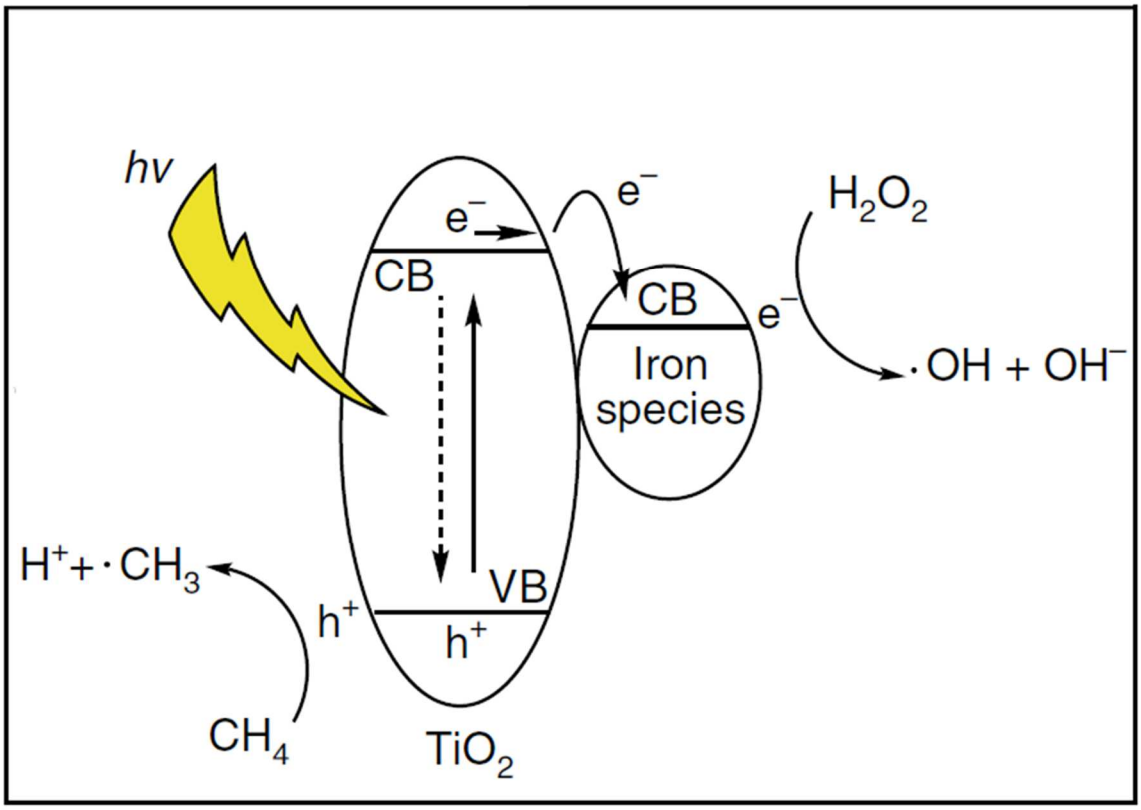

Figure 9. Reaction steps in methane oxidation with H_2O_2 over FeO_x/TiO_2 (from Ref. [58])

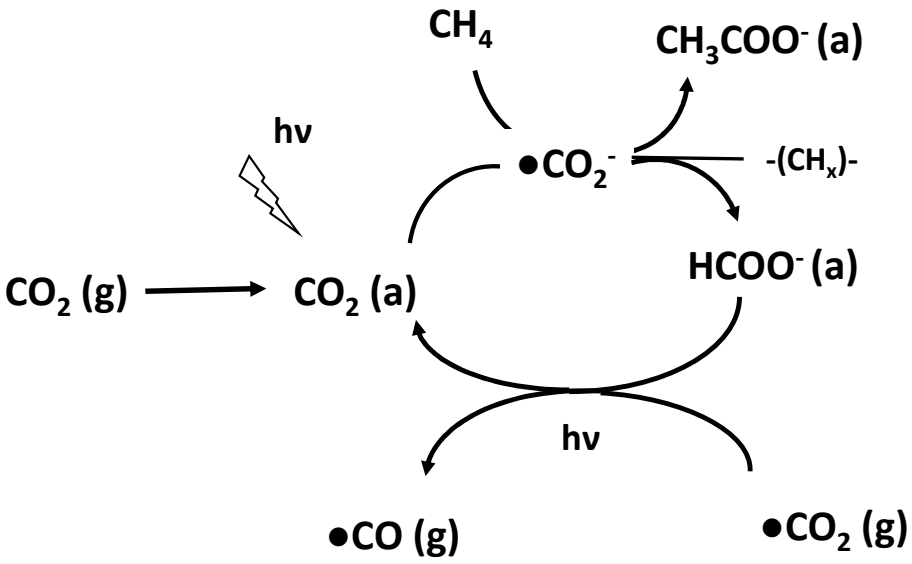

Figure 10. Reaction mechanism in the photoreduction of CO_2 with CH_4 over ZrO_2 (from Ref. [71])

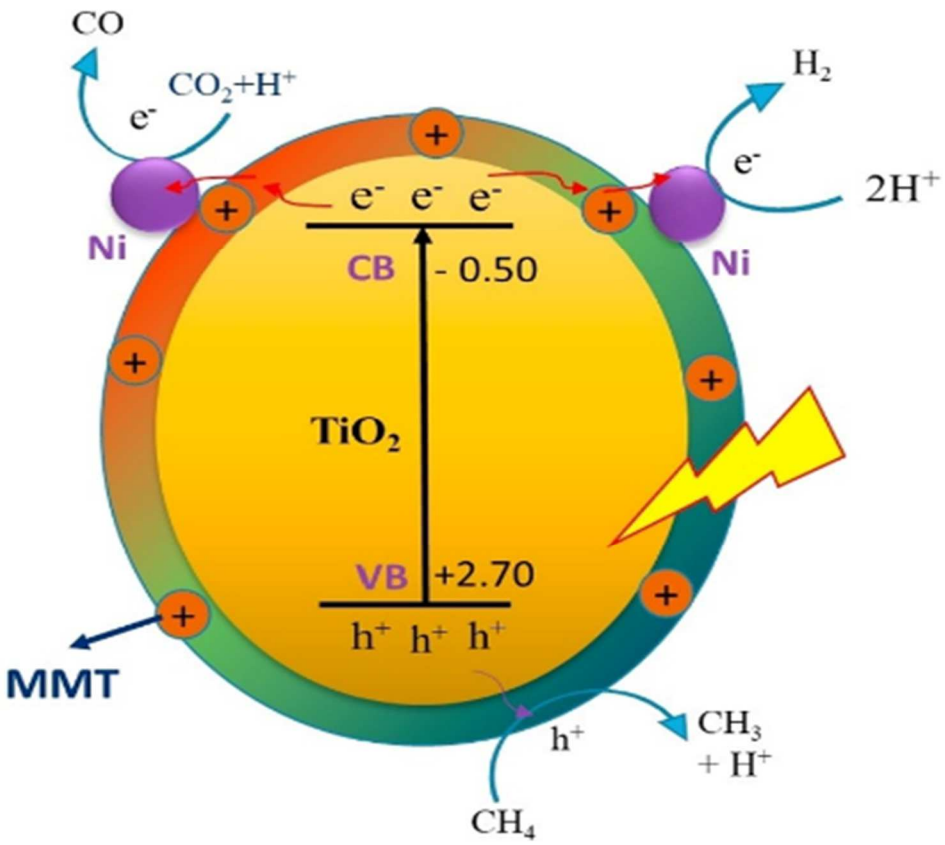

Figure 11. Schematic of photocatalytic DRM over Ni-MMT/TiO_2 composite (from Ref. [76])

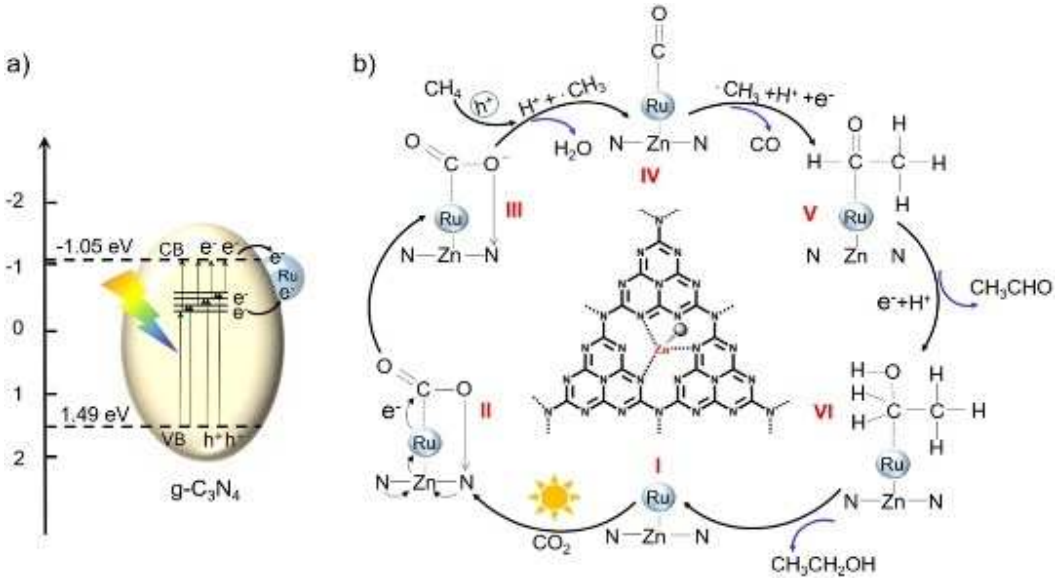

Figure 12. Schematic of (a) the band structure induced charge transfer process and (b) surface reaction mechanism for the photocatalytic DRM (from Ref. [82])

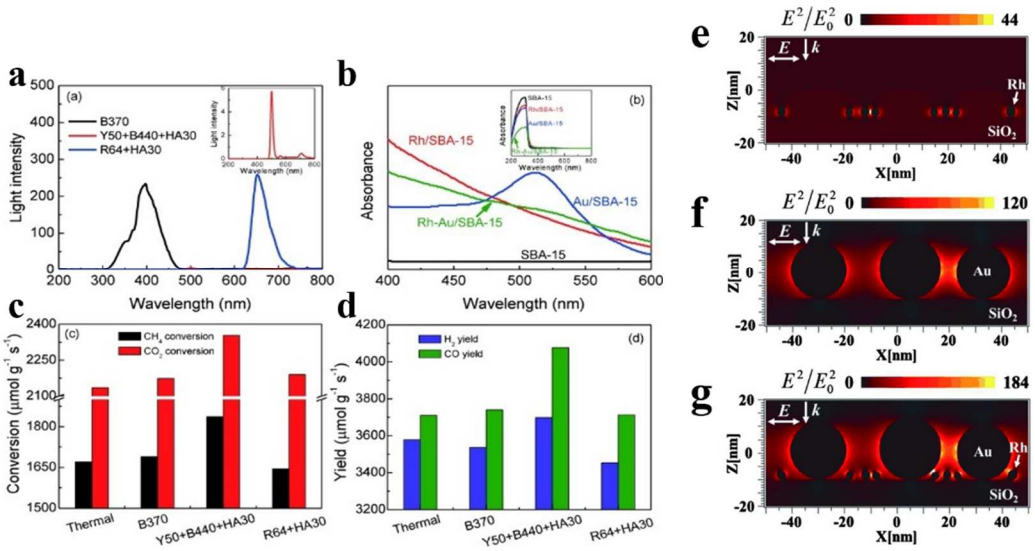

Figure 13. (a) Incident light with different wavelength region over filters. (b) UV/Vis spectra of catalysts. (c) methane and carbon dioxide conversions and (d) carbon monoxide and hydrogen yield counterparts under various irradiation conditions. (e-g) electric field distribution of the catalyst under visible-light excitation of 530 nm, the color scale bar shows the electric field enhancement. (e) Rh/SBA-15. (f) Au/SBA-15. (g) Rh-Au/SBA-15 (from Ref. [44]).

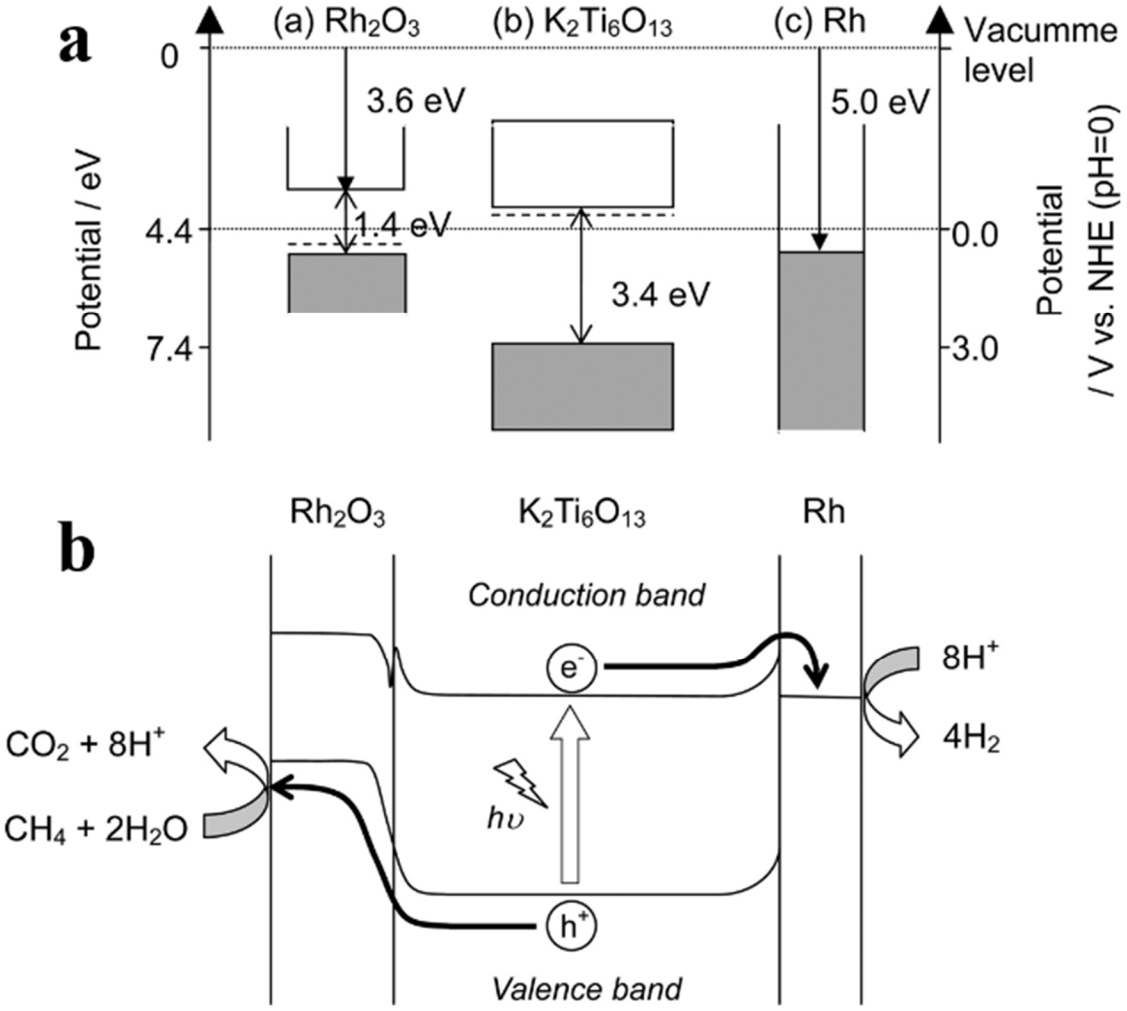

Figure 14. (a) Band structure of various components and (b) proposed mechanism in the photocatalytic SRM over the Rh loaded $K_2Ti_6O_{13}$ prepared by the photo-deposition method (from Ref. [97])

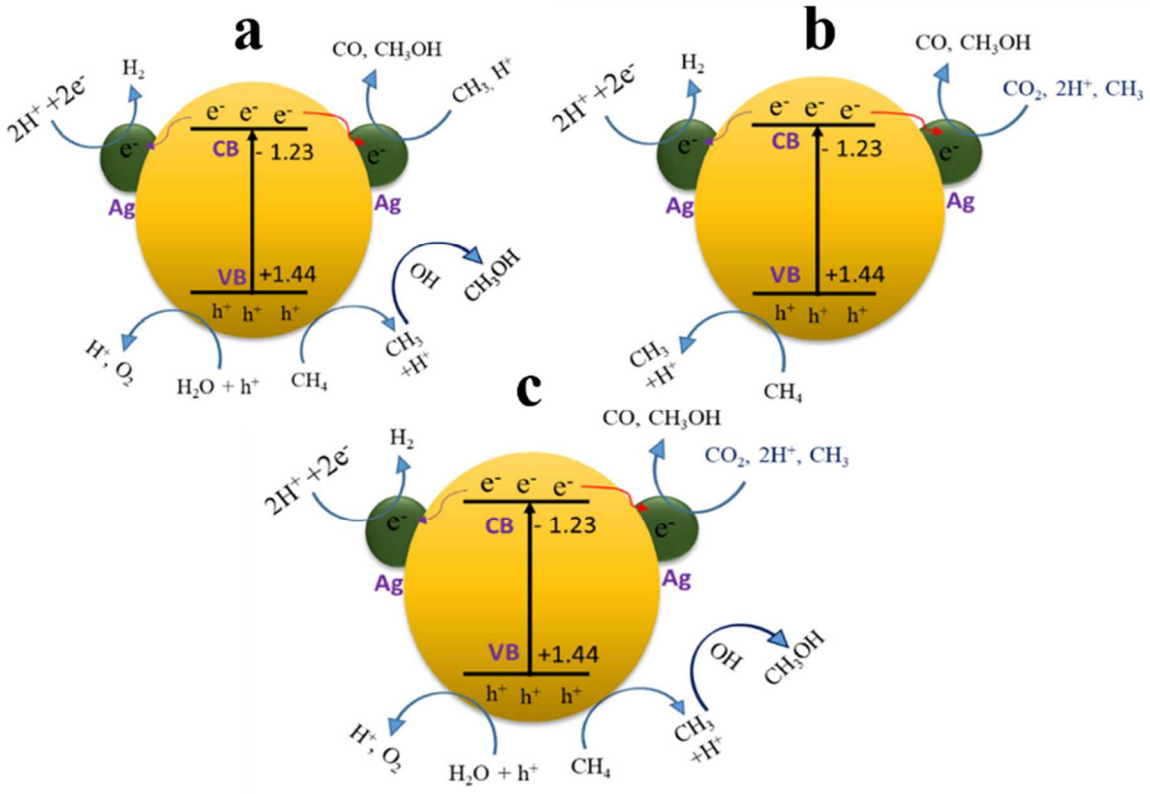

Figure 15. Proposed scheme for photocatalytic (a) SRM, (b) DRM and (c) BRM over Ag/pg-C_3N_4 (from Ref. [98])

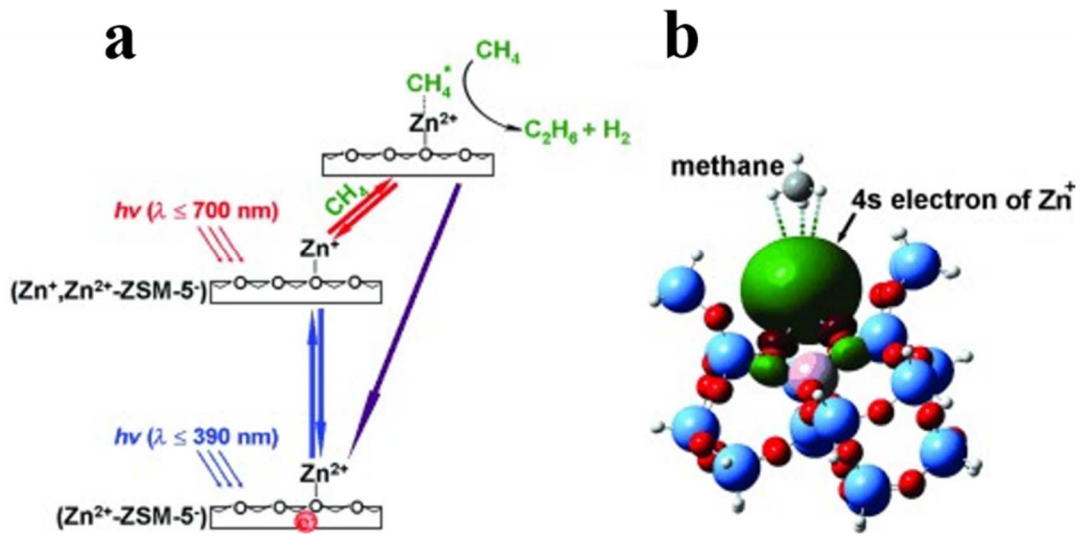

Figure 16. (a) Proposed photocatalytic mechanism over Zn-ZSM-5 catalysts and (b) geometry of the adsorbed methane molecule attracted by the Zn^+ active site (red: O, blue: Si, pink: Al, gray: C, white: H, and green: the 4s electron of Zn^+) (from Ref. [106])

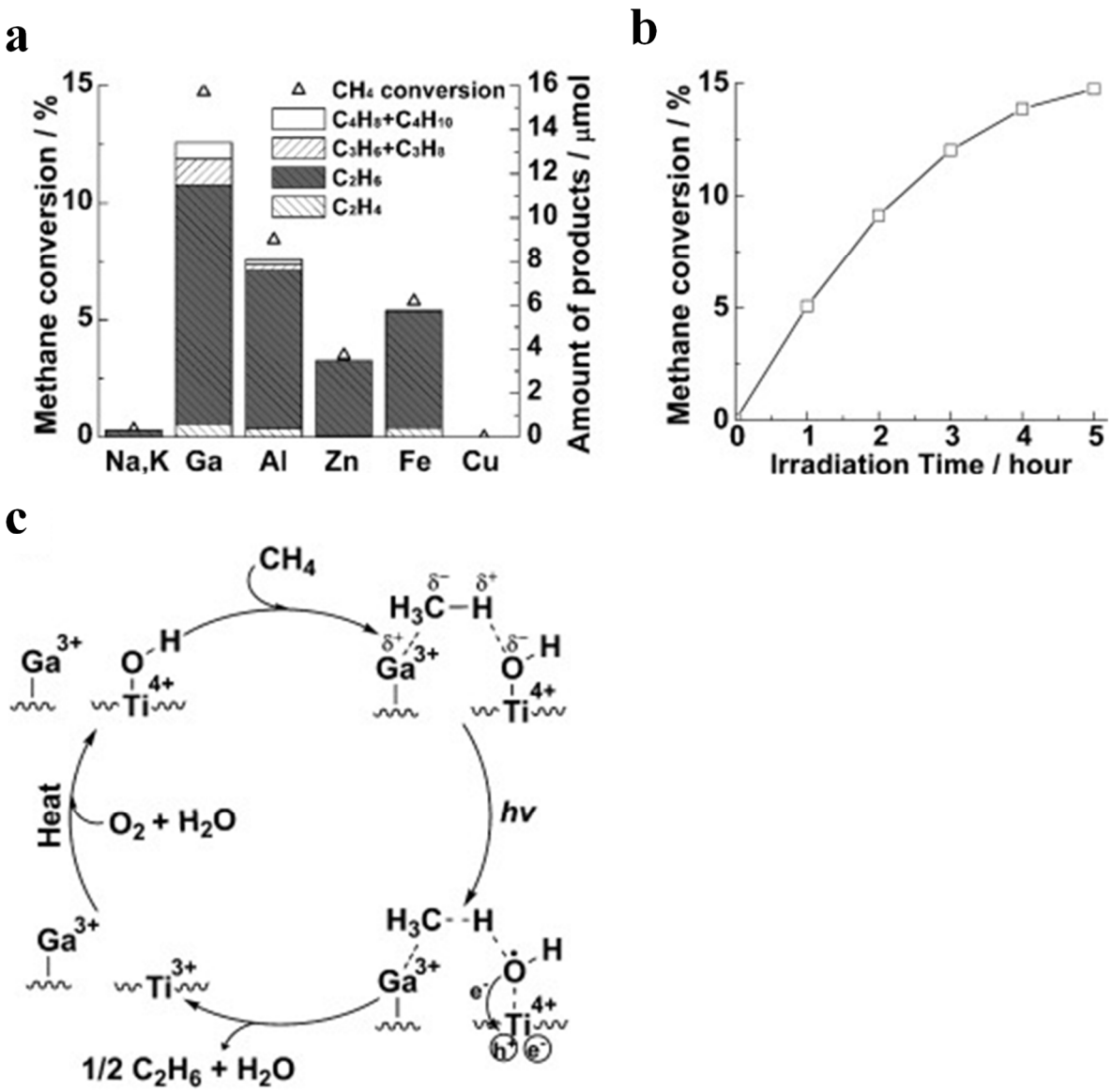

Figure 17. (a) Photocatalytic NOCM performance of various metal ions modified ETS-10, (b) methane conversion and (c) proposed reaction mechanism over Ga^{3+} modified ETS-10 in photocatalytic NOCM (from Ref. [48])

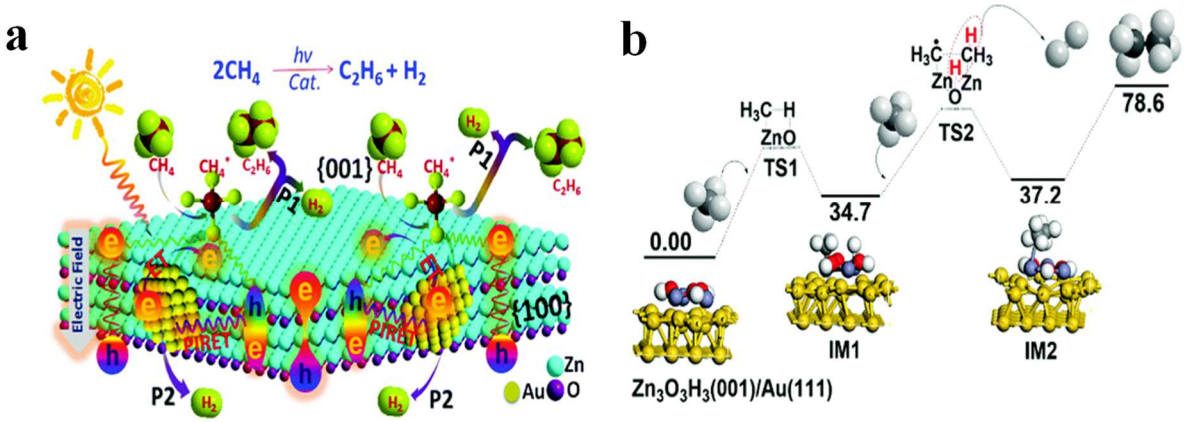

Figure 18. (a) Schematic description of the idealized Au/ZnO (001) nanocomposite for the dehydrogenative coupling of methane into ethane. (b) Potential energy diagram for the methane coupling reaction on Au/ZnO (001) clusters (energy in $kJ \cdot mol^{-1}$) (from Ref. [107]).

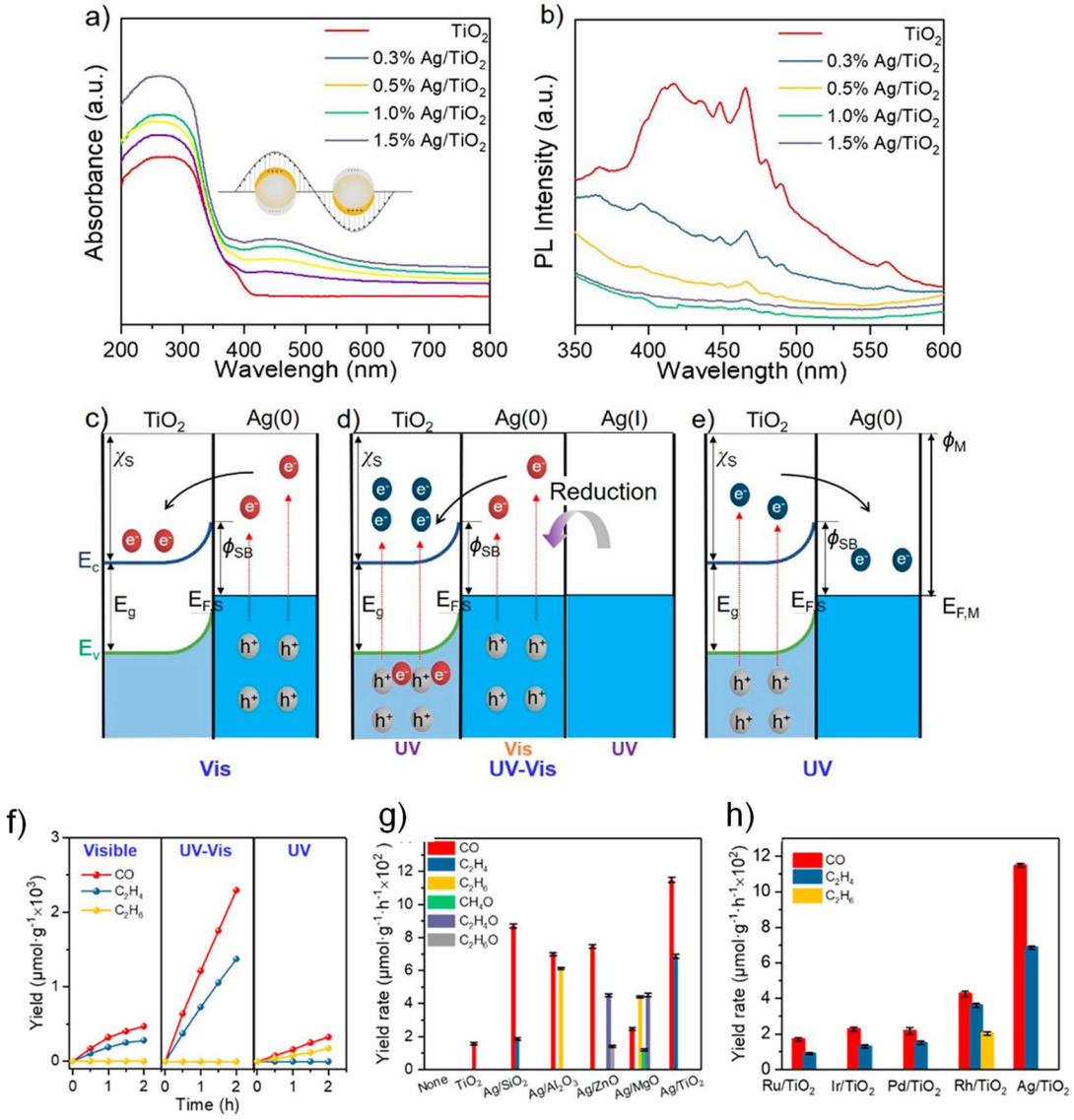

Figure 19. (a) UV–visible spectra and (b) PL spectra of Ag/TiO_2 photocatalysts. (c–e) Schematic illustration of the proposed electron transfer process involved in Ag/TiO_2 photocatalyst under different light source. (f) Photocatalytic CH_4 and CO_2 conversions over 1% Ag/TiO_2 under different light source. (g, h) The effect of the type of (g) supports and (h) active metals on photocatalytic performance, under simulated solar irradiation (from Ref. [108])

.

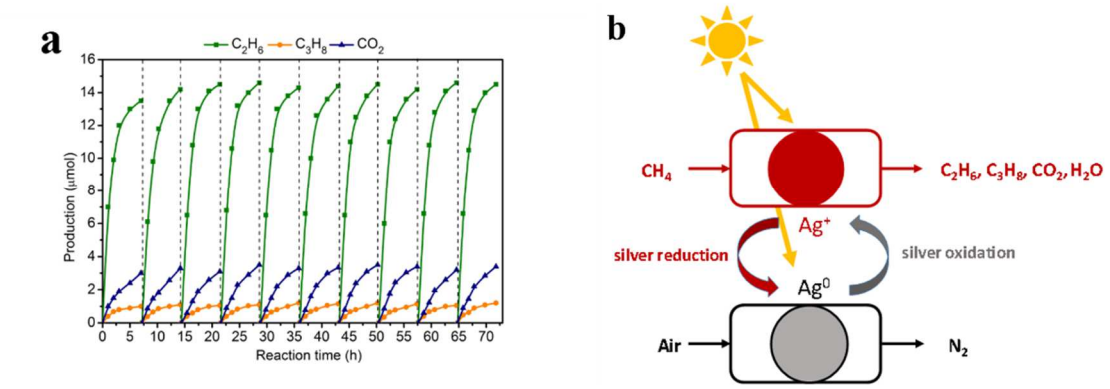

Figure 20. (a) Reaction–regeneration cycles in methane photochemical coupling on Ag–HPW/TiO_2. The solid lines are guides to the eye. Dashed lines represent nanocomposite regeneration and (b) Schematic description of photochemical looping process (from Ref. [110])

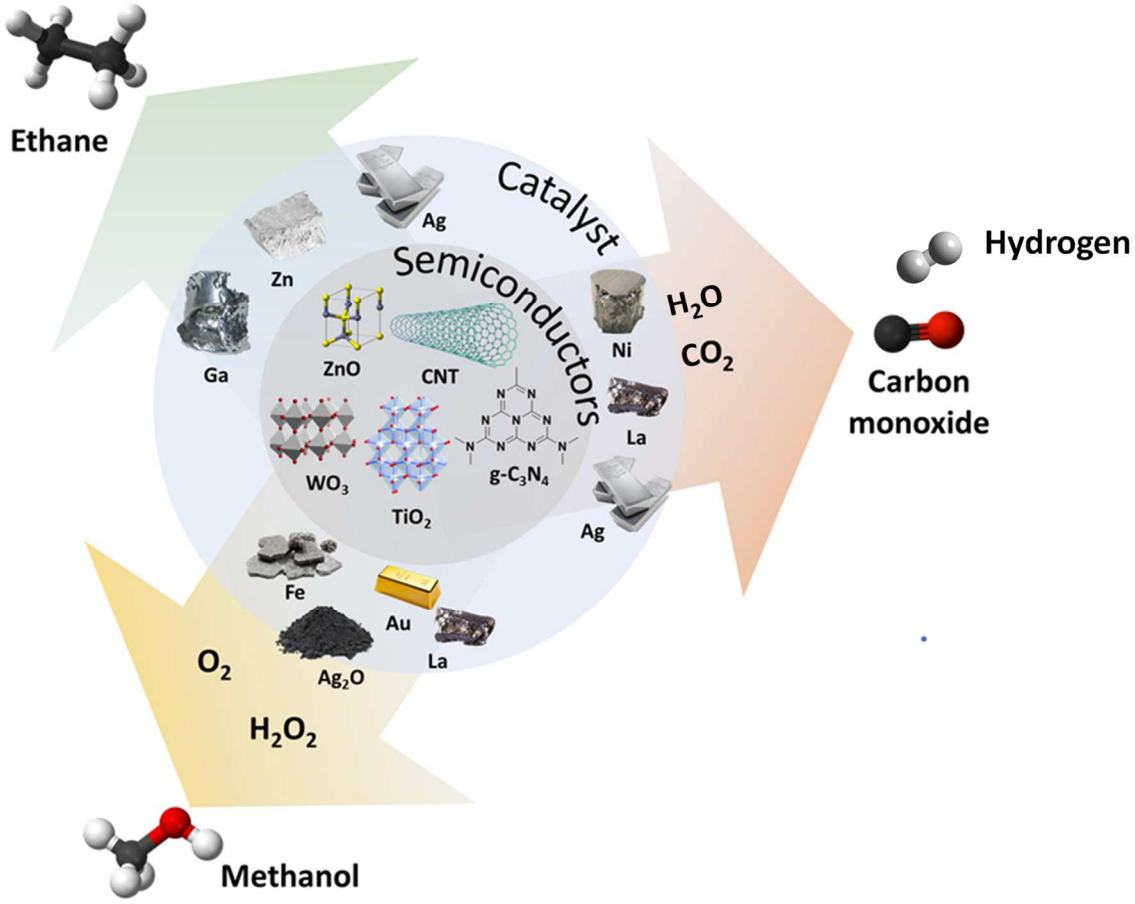

Figure 21. Semiconductors and co-catalysts for three major routes of methane photocatalytic conversion.

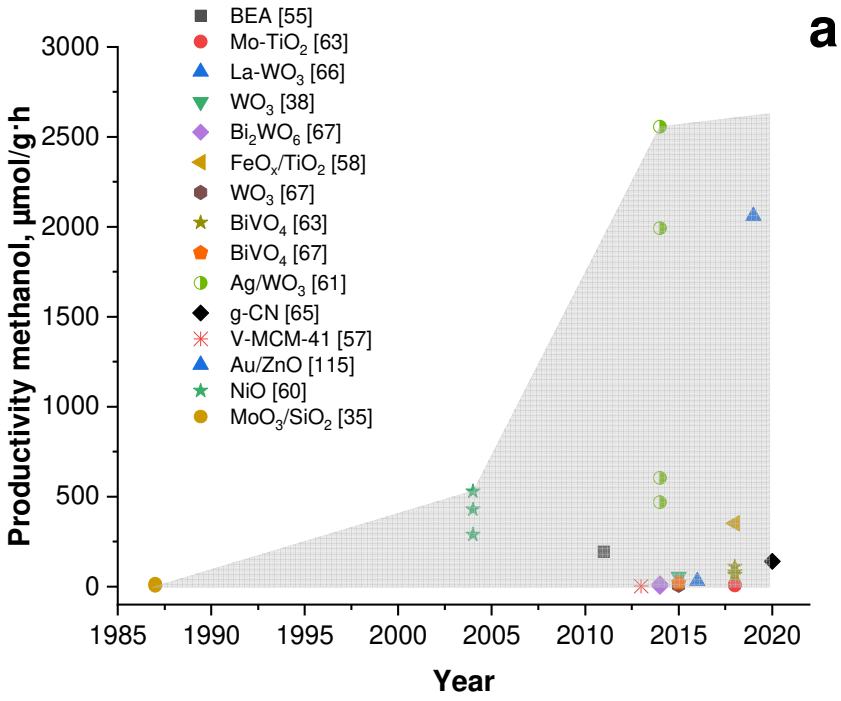
a
BEA [55]
Mo-TiO2 [63]
La-WO3 [66]
WO3 [38]
Bi2WO6 [67]
FeOx/TiO2 [58]
WO3 [67]
BiVO4 [63]
BiVO4 [67]
Ag/WO3 [61]
g-CN [65]
V-MCM-41 [57]
Au/ZnO [115]
NiO [60]
MoO3/SiO2 [35]
Productivity methanol, µmol/g·h
3000
2500
2000
1500
1000
500
0
1985
1990
1995
2000
2005
2010
2015
2020
Year

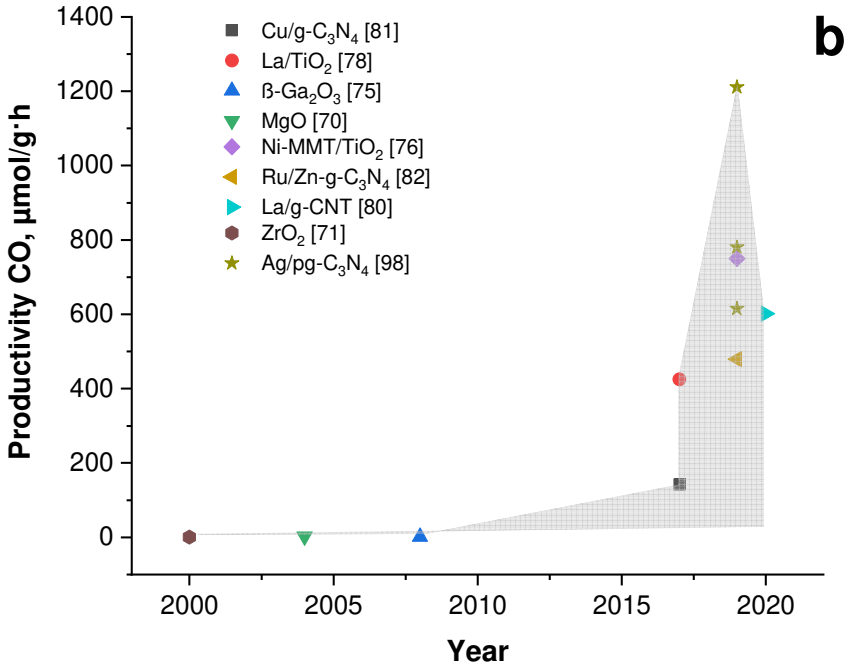
b
Cu/g-C3N4 [81]
La/TiO2 [78]
ß-Ga2O3 [75]
MgO [70]
Ni-MMT/TiO2 [76]
Ru/Zn-g-C3N4 [82]
La/g-CNT [80]
ZrO2 [71]
Ag/pg-C3N4 [98]
Productivity CO, µmol/g·h
1400
1200
1000
800
600
400
200
0
2000
2005
2010
2015
2020
Year

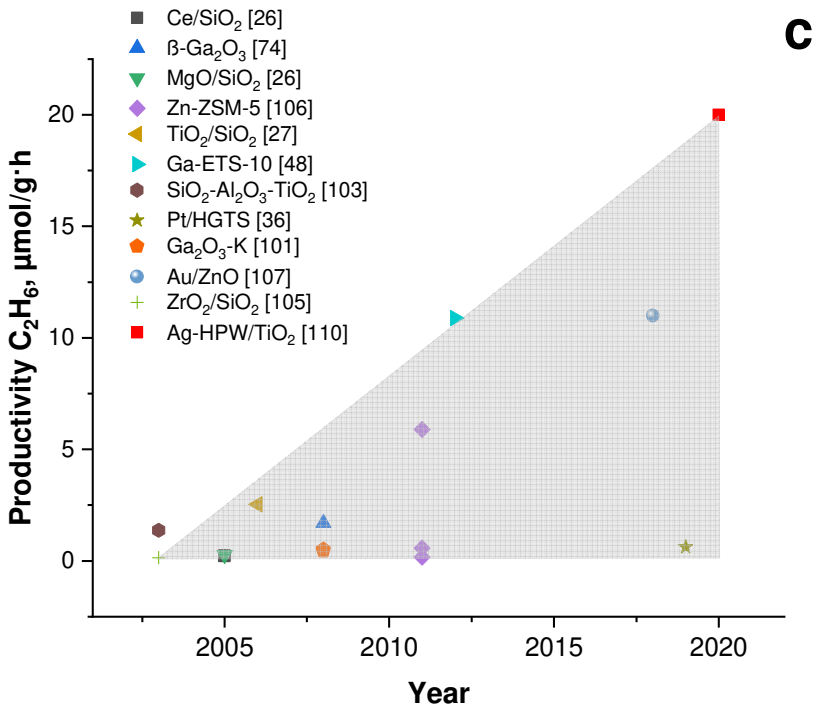

Figure 22. Evolution with time of reported methanol (a), CO (b) and ethane (c) productivities in photocatalytic methane POM, methane reforming and methane coupling occurring at low temperatures

Reference

[1] E. McFarland, Unconventional chemistry for unconventional natural gas, Science 338 (2012) 341–342. https://doi.org/10.1126/science.1226840.

[2] E. V. Kondratenko, T. Peppel, D. Seeburg, V.A. Kondratenko, N. Kalevaru, A. Martin, S. Wohlrab, Methane conversion into different hydrocarbons or oxygenates: Current status and future perspectives in catalyst development and reactor operation, Catal. Sci. Technol. 7 (2017) 366–381. https://doi.org/10.1039/c6cy01879c.

[3] R. Horn, R. Schlögl, Methane Activation by Heterogeneous Catalysis, Catal. Letters. 145 (2015) 23–39. https://doi.org/10.1007/s10562-014-1417-z.

[4] P. Schwach, X. Pan, X. Bao, Direct Conversion of Methane to Value-Added Chemicals over Heterogeneous Catalysts: Challenges and Prospects, Chem. Rev. 117 (2017) 8497–8520. https://doi.org/10.1021/acs.chemrev.6b00715.

[5] G.E. Johnson, W.A. Decker, A.J. Forney, J.H. Field, Hydrogen cyanide produced from coal and ammonia, Ind. Eng. Chem. Process Des. Dev. 7 (1968) 137–143. https://doi.org/10.1021/i260025a027.

[6] J.J. Spivey, G. Hutchings, Catalytic aromatization of methane, Chem. Soc. Rev. 43 (2014) 792–803. https://doi.org/10.1039/c3cs60259a.

[7] M.H. Ab Rahim, M.M. Forde, R.L. Jenkins, C. Hammond, Q. He, N. Dimitratos, J.A. Lopez-Sanchez, A.F. Carley, S.H. Taylor, D.J. Willock, D.M. Murphy, C.J. Kiely, G.J. Hutchings, Oxidation of methane to methanol with hydrogen peroxide using supported gold-palladium alloy nanoparticles, Angew. Chemie - Int. Ed. 52 (2013) 1280–1284. https://doi.org/10.1002/anie.201207717.

[8] C. Hammond, M.M. Forde, M.H. Ab Rahim, A. Thetford, Q. He, R.L. Jenkins, N. Dimitratos, J.A. Lopez-Sanchez, N.F. Dummer, D.M. Murphy, A.F. Carley, S.H. Taylor, D.J. Willock, E.E. Stangland, J. Kang, H. Hagen, C.J. Kiely, G.J. Hutchings, Direct catalytic conversion of methane to methanol in an aqueous medium by using

copper-promoted Fe-ZSM-5, Angew. Chemie - Int. Ed. 51 (2012) 5129–5133. https://doi.org/10.1002/anie.201108706.

[9] P. Tomkins, M. Ranocchiari, J.A. Van Bokhoven, Direct Conversion of Methane to Methanol under Mild Conditions over Cu-Zeolites and beyond, Acc. Chem. Res. 50 (2017) 418–425. https://doi.org/10.1021/acs.accounts.6b00534.

[10] N. Agarwal, S.J. Freakley, R.U. McVicker, S.M. Althahban, N. Dimitratos, Q. He, D.J. Morgan, R.L. Jenkins, D.J. Willock, S.H. Taylor, C.J. Kiely, G.J. Hutchings, Aqueous Au-Pd colloids catalyze selective CH_4 oxidation to CH_3OH with O_2 under mild conditions, Science 358 (2017) 223–227. https://doi.org/10.1126/science.aan6515.

[11] M.H. Groothaert, P.J. Smeets, B.F. Sels, P.A. Jacobs, R.A. Schoonheydt, Selective Oxidation of Methane by the Bis(μ-oxo)dicopper Core Stabilized on ZSM-5 and Mordenite Zeolites, J. Am. Chem. Soc. 127 (2005) 1394–1395. https://doi.org/10.1021/ja047158u.

[12] S. Grundner, M.A.C. Markovits, G. Li, M. Tromp, E.A. Pidko, E.J.M. Hensen, A. Jentys, M. Sanchez-Sanchez, J.A. Lercher, Single-site trinuclear copper oxygen clusters in mordenite for selective conversion of methane to methanol, Nat. Commun. 6 (2015). https://doi.org/10.1038/ncomms8546.

[13] V.L. Sushkevich, D. Palagin, M. Ranocchiari, J.A. van Bokhoven, Selective anaerobic oxidation of methane enables direct synthesis of methanol, Science 356 (2017) 523–527. https://doi.org/10.1126/science.aam9035.

[14] D. Palagin, V.L. Sushkevich, J.A. Van Bokhoven, Water Molecules Facilitate Hydrogen Release in Anaerobic Oxidation of Methane to Methanol over Cu/Mordenite, ACS Catal. 9 (2019) 10365–10374. https://doi.org/10.1021/acscatal.9b02702.

[15] J. Zhu, V.L. Sushkevich, A.J. Knorpp, M.A. Newton, S.C.M. Mizuno, T. Wakihara, T. Okubo, Z. Liu, J.A. Van Bokhoven, Cu-Erionite Zeolite Achieves High Yield in Direct

Oxidation of Methane to Methanol by Isothermal Chemical Looping, Chem. Mater. 32 (2020) 1448–1453. https://doi.org/10.1021/acs.chemmater.9b04223.

[16] P. Tang, Q. Zhu, Z. Wu, D. Ma, Methane activation: the past and future, Energy Environ. Sci. 7 (2014) 2580–2591. https://doi.org/10.1039/C4EE00604F.

[17] X. Meng, X. Cui, N.P. Rajan, L. Yu, D. Deng, X. Bao, Direct Methane Conversion under Mild Condition by Thermo-, Electro-, or Photocatalysis, Chem. 5 (2019) 2296–2325. https://doi.org/10.1016/j.chempr.2019.05.008.

[18] L. Sun, Y. Wang, N. Guan, L. Li, Methane Activation and Utilization: Current Status and Future Challenges, Energy Technol. (2019). https://doi.org/10.1002/ente.201900826.

[19] B. Wang, S. Albarracín-Suazo, Y. Pagán-Torres, E. Nikolla, Advances in methane conversion processes, Catal. Today. 285 (2017) 147–158. https://doi.org/10.1016/j.cattod.2017.01.023.

[20] F. Roudesly, J. Oble, G. Poli, Metal-catalyzed CH activation/functionalization: The fundamentals, J. Mol. Catal. A Chem. 426 (2017) 275–296. https://doi.org/10.1016/j.molcata.2016.06.020.

[21] L. Yuliati, H. Yoshida, Photocatalytic conversion of methane, Chem. Soc. Rev. 37 (2008) 1592. https://doi.org/10.1039/b710575b.

[22] X. Cai, Y.H. Hu, Advances in catalytic conversion of methane and carbon dioxide to highly valuable products, Energy Sci. Eng. 7 (2019) 4–29. https://doi.org/10.1002/ese3.278.

[23] L. Pan, M. Ai, C. Huang, L. Yin, X. Liu, R. Zhang, S. Wang, Z. Jiang, X. Zhang, J.J. Zou, W. Mi, Manipulating spin polarization of titanium dioxide for efficient photocatalysis, Nat. Commun. 11 (2020). https://doi.org/10.1038/s41467-020-14333-w.

[24] U.G. Akpan, B.H. Hameed, Parameters affecting the photocatalytic degradation of dyes

using TiO_2-based photocatalysts: A review, J. Hazard. Mater. 170 (2009) 520–529. https://doi.org/10.1016/j.jhazmat.2009.05.039.

[25] Q. Li, H. Yue, C. Liu, K. Ma, S. Zhong, B. Liang, S. Tang, A Photocatalytic Transformation Realized by Pd/TiO_2 Particle Size Modulation: from Oxidative Ethane Dehydrogenation to Direct Ethane Dehydrogenation, Chem. Eng. J. 395 (2020) 125120. https://doi.org/10.1016/j.cej.2020.125120.

[26] L. Yuliati, T. Hattori, H. Yoshida, Highly dispersed magnesium oxide species on silica as photoactive sites for photoinduced direct methane coupling and photoluminescence, Phys. Chem. Chem. Phys. 7 (2005) 195–201. https://doi.org/10.1039/b410089a.

[27] L. Yuliati, H. Itoh, H. Yoshida, Preparation of isolated highly dispersed titanium oxides on silica by sol-gel method for photocatalytic non-oxidative direct methane coupling, Stud. Surf. Sci. Catal. 162 (2006) 961–968. https://doi.org/10.1016/S0167-2991(06)81003-7.

[28] C.E. Taylor, R.P. Noceti, New developments in the photocatalytic conversion of methane to methanol, Catal. Today. 55 (2000) 259–267. https://doi.org/10.1016/S0920-5861(99)00244-8.

[29] E. Kowalska, Z. Wei, M. Janczarek, Band-gap Engineering of Photocatalysts: Surface Modification versus Doping, in: Visible Light. Photocatal., Wiley-VCH Verlag GmbH & Co. KGaA, Weinheim, Germany, 2018: pp. 447–484. https://doi.org/10.1002/9783527808175.ch16.

[30] X. Yu, V. De Waele, A. Löfberg, V. Ordomsky, A.Y.A.Y. Khodakov, V. De Waele, A. Löfberg, V. Ordomsky, A.Y.A.Y. Khodakov, Selective photocatalytic conversion of methane into carbon monoxide over zinc-heteropolyacid-titania nanocomposites, Nat. Commun. 10 (2019) 700. https://doi.org/10.1038/s41467-019-08525-2.

[31] G. Marcì, E.I. García-Lõpez, L. Palmisano, Heteropolyacid-based materials as

heterogeneous photocatalysts, Eur. J. Inorg. Chem. (2014) 21–35. https://doi.org/10.1002/ejic.201300883.

[32] M.S. Nasir, G. Yang, I. Ayub, S. Wang, W. Yan, Tin diselinide a stable co-catalyst coupled with branched TiO_2 fiber and g-C_3N_4 quantum dots for photocatalytic hydrogen evolution, Appl. Catal. B Environ. 270 (2020) 118900. https://doi.org/10.1016/j.apcatb.2020.118900.

[33] Q. Xu, L. Zhang, B. Cheng, J. Fan, J. Yu, S-Scheme Heterojunction Photocatalyst, Chem. 6 (2020) 1543–1559. https://doi.org/10.1016/j.chempr.2020.06.010.

[34] B. Han, W. Wei, L. Chang, P. Cheng, Y.H. Hu, Efficient Visible Light Photocatalytic CO_2 Reforming of CH_4, ACS Catal. 6 (2016) 494–497. https://doi.org/10.1021/acscatal.5b02653.

[35] M.D. Ward, J.F. Brazdil, S.P. Mehandru, A.B. Anderson, Methane photoactivation on copper molybdate. An experimental and theoretical study, J. Phys. Chem. 91 (1987) 6515–6521. https://doi.org/10.1021/j100310a019.

[36] S. Wu, X. Tan, J. Lei, H. Chen, L. Wang, J. Zhang, Ga-Doped and Pt-Loaded Porous TiO_2 –SiO_2 for Photocatalytic Nonoxidative Coupling of Methane, J. Am. Chem. Soc. 141 (2019) 6592–6600. https://doi.org/10.1021/jacs.8b13858.

[37] Y. Ben-Shahar, F. Scotognella, I. Kriegel, L. Moretti, G. Cerullo, E. Rabani, U. Banin, Optimal metal domain size for photocatalysis with hybrid semiconductor-metal nanorods, Nat. Commun. 7 (2016) 1–7. https://doi.org/10.1038/ncomms10413.

[38] K. Villa, S. Murcia-López, T. Andreu, J.R. Morante, Mesoporous WO_3 photocatalyst for the partial oxidation of methane to methanol using electron scavengers, Appl. Catal. B Environ. 163 (2015) 150–155. https://doi.org/10.1016/j.apcatb.2014.07.055.

[39] S. Mukherjee, F. Libisch, N. Large, O. Neumann, L. V. Brown, J. Cheng, J.B. Lassiter, E.A. Carter, P. Nordlander, N.J. Halas, Hot electrons do the impossible: Plasmon-

induced dissociation of H_2 on Au, Nano Lett. 13 (2013) 240–247. https://doi.org/10.1021/nl303940z.

[40] P. Christopher, H. Xin, S. Linic, Visible-light-enhanced catalytic oxidation reactions on plasmonic silver nanostructures, Nat. Chem. 3 (2011) 467–472. https://doi.org/10.1038/nchem.1032.

[41] A. Marimuthu, J. Zhang, S. Linic, Tuning selectivity in propylene epoxidation by plasmon mediated photo-switching of Cu oxidation state, Science (80-.). 340 (2013) 1590–1593. https://doi.org/10.1126/science.1231631.

[42] H. Liu, X. Meng, T.D. Dao, L. Liu, P. Li, G. Zhao, T. Nagao, L. Yang, J. Ye, Light assisted CO2 reduction with methane over SiO_2 encapsulated Ni nanocatalysts for boosted activity and stability, J. Mater. Chem. A. 5 (2017) 10567–10573. https://doi.org/10.1039/c7ta00704c.

[43] B. László, K. Baán, E. Varga, A. Oszkó, A. Erdőhelyi, Z. Kónya, J. Kiss, Photo-induced reactions in the CO_2-methane system on titanate nanotubes modified with Au and Rh nanoparticles, Appl. Catal. B Environ. 199 (2016) 473–484. https://doi.org/10.1016/j.apcatb.2016.06.057.

[44] H. Liu, X. Meng, T.D. Dao, H. Zhang, P. Li, K. Chang, T. Wang, M. Li, T. Nagao, J. Ye, Conversion of Carbon Dioxide by Methane Reforming under Visible-Light Irradiation: Surface-Plasmon-Mediated Nonpolar Molecule Activation, Angew. Chemie - Int. Ed. 54 (2015) 11545–11549. https://doi.org/10.1002/anie.201504933.

[45] G. Baffou, R. Quidant, Thermo-plasmonics: using metallic nanostructures as nano-sources of heat, Laser Photon. Rev. 7 (2013) 171–187. https://doi.org/10.1002/lpor.201200003.

[46] G. Baffou, R. Quidant, Nanoplasmonics for chemistry, Chem. Soc. Rev. 43 (2014) 3898. https://doi.org/10.1039/c3cs60364d.

[47] S. Linic, U. Aslam, C. Boerigter, M. Morabito, Photochemical transformations on plasmonic metal nanoparticles, Nat. Mater. 14 (2015) 567–576. https://doi.org/10.1038/nmat4281.

[48] L. Li, Y.Y. Cai, G.D. Li, X.Y. Mu, K.X. Wang, J.S. Chen, Synergistic effect on the photoactivation of the methane C-H bond over Ga^{3+}-modified ETS-10, Angew. Chemie - Int. Ed. 51 (2012) 4702–4706. https://doi.org/10.1002/anie.201200045.

[49] H. Song, X. Meng, Z. Wang, H. Liu, J. Ye, Solar-Energy-Mediated Methane Conversion, Joule. 3 (2019) 1606–1636. https://doi.org/10.1016/j.joule.2019.06.023.

[50] I. Grčić, J. Marčec, L. Radetić, A.-M. Radovan, I. Melnjak, I. Jajčinović, I. Brnardić, Ammonia and methane oxidation on TiO_2 supported on glass fiber mesh under artificial solar irradiation, Environ. Sci. Pollut. Res. (2020). https://doi.org/10.1007/s11356-020-09561-y.

[51] X. Chen, Y. Li, X. Pan, D. Cortie, X. Huang, Z. Yi, Photocatalytic oxidation of methane over silver decorated zinc oxide nanocatalysts, Nat. Commun. 7 (2016). https://doi.org/10.1038/ncomms12273.

[52] R. de Richter, T. Ming, P. Davies, W. Liu, S. Caillol, Removal of non-CO_2 greenhouse gases by large-scale atmospheric solar photocatalysis, Prog. Energy Combust. Sci. 60 (2017) 68–96. https://doi.org/10.1016/j.pecs.2017.01.001.

[53] S.L. Kaliaguine, B.N. Shelimov, V.B. Kazansky, Reactions of methane and ethane with hole centers O^-, J. Catal. 55 (1978) 384–393. https://doi.org/10.1016/0021-9517(78)90225-7.

[54] X. Chen, Y. Li, X. Pan, D. Cortie, X. Huang, Z. Yi, Photocatalytic oxidation of methane over silver decorated zinc oxide nanocatalysts, Nat. Commun. 7 (2016) 1–8. https://doi.org/10.1038/ncomms12273.

[55] F. Sastre, V. Fornés, A. Corma, H. García, Selective, room-temperature transformation

of methane to C1 oxygenates by deep UV photolysis over zeolites, J. Am. Chem. Soc. 133 (2011) 17257–17261. https://doi.org/10.1021/ja204559z.

[56] W. Zhou, X. Qiu, Y. Jiang, Y. Fan, S. Wei, D. Han, L. Niu, Z. Tang, Highly selective aerobic oxidation of methane to methanol over gold decorated zinc oxide: Via photocatalysis, J. Mater. Chem. A. 8 (2020) 13277–13284. https://doi.org/10.1039/d0ta02793f.

[57] Y. Hu, M. Anpo, C. Wei, Effect of the local structures of v-oxides in MCM-41 on the photocatalytic properties for the partial oxidation of methane to methanol, J. Photochem. Photobiol. A Chem. 264 (2013) 48–55. https://doi.org/10.1016/j.jphotochem.2013.05.005.

[58] J. Xie, R. Jin, A. Li, Y. Bi, Q. Ruan, Y. Deng, Y. Zhang, S. Yao, G. Sankar, D. Ma, J. Tang, Highly selective oxidation of methane to methanol at ambient conditions by titanium dioxide-supported iron species, Nat. Catal. 1 (2018) 889–896. https://doi.org/10.1038/s41929-018-0170-x.

[59] X. Chen, S. Li, Photooxidation of methane to methanol by molecular oxygen on water-preadsorbed porous TiO_2-based catalysts, Chem. Lett. (2000) 314–315. https://doi.org/10.1246/cl.2000.314.

[60] M.A. Gondal, A. Hameed, Z.H. Yamani, A. Arfaj, Photocatalytic transformation of methane into methanol under UV laser irradiation over WO_3, TiO_2 and NiO catalysts, Chem. Phys. Lett. 392 (2004) 372–377. https://doi.org/10.1016/j.cplett.2004.05.092.

[61] A. Hameed, I.M.I. Ismail, M. Aslam, M.A. Gondal, Photocatalytic conversion of methane into methanol: Performance of silver impregnated WO_3, Appl. Catal. A Gen. 470 (2014) 327–335. https://doi.org/10.1016/j.apcata.2013.10.045.

[62] J. Du, W. Chen, G. Wu, Y. Song, X. Dong, G. Li, J. Fang, W. Wei, Y. Sun, Evoked methane photocatalytic conversion to C_2 oxygenates over ceria with oxygen vacancy,

Catalysts. 10 (2020). https://doi.org/10.3390/catal10020196.

[63] W. Zhu, M. Shen, G. Fan, A. Yang, J.R. Meyer, Y. Ou, B. Yin, J. Fortner, M. Foston, Z. Li, Z. Zou, B. Sadtler, Facet-Dependent Enhancement in the Activity of Bismuth Vanadate Microcrystals for the Photocatalytic Conversion of Methane to Methanol, ACS Appl. Nano Mater. 1 (2018) 6683–6691. https://doi.org/10.1021/acsanm.8b01490.

[64] Y. Zeng, H.C. Liu, J.S. Wang, X.Y. Wu, S.L. Wang, Synergistic photocatalysis-Fenton reaction for selective conversion of methane to methanol at room temperature, Catal. Sci. Technol. 10 (2020) 2329–2332. https://doi.org/10.1039/d0cy00028k.

[65] S. Shi, Z. Sun, C. Bao, T. Gao, Y.H. Hu, The special route toward conversion of methane to methanol on a fluffy metal-free carbon nitride photocatalyst in the presence of H_2O_2, Int. J. Energy Res. (2020). https://doi.org/10.1002/er.5088.

[66] K. Villa, S. Murcia-López, T. Andreu, J.R. Morante, On the role of WO_3 surface hydroxyl groups for the photocatalytic partial oxidation of methane to methanol, Catal. Commun. 58 (2015) 200–203. https://doi.org/10.1016/j.catcom.2014.09.025.

[67] S. Murcia-López, K. Villa, T. Andreu, J.R. Morante, Improved selectivity for partial oxidation of methane to methanol in the presence of nitrite ions and $BiVO_4$ photocatalyst, Chem. Commun. 51 (2015) 7249–7252. https://doi.org/10.1039/c5cc00978b.

[68] Y. Zhou, L. Zhang, W. Wang, Direct functionalization of methane into ethanol over copper modified polymeric carbon nitride via photocatalysis, Nat. Commun. 10 (2019). https://doi.org/10.1038/s41467-019-08454-0.

[69] Y. Kohno, T. Tanaka, T. Funabiki, S. Yoshida, Photoreduction of Carbon Dioxide with Methane over ZrO_2, Chem. Lett. 26 (1997) 993–994. https://doi.org/10.1246/cl.1997.993.

[70] K. Teramura, T. Tanaka, H. Ishikawa, Y. Kohno, T. Funabiki, Photocatalytic

Reduction of CO_2 to CO in the Presence of H_2 or CH_4 as a Reductant over MgO, J. Phys. Chem. B. 108 (2004) 346–354. https://doi.org/10.1021/jp0362943.

[71] Y. Kohno, T. Tanaka, T. Funabiki, S. Yoshida, Reaction mechanism in the photoreduction of CO_2 with CH_4 over ZrO_2, Phys. Chem. Chem. Phys. 2 (2000) 5302–5307. https://doi.org/10.1039/b005315p.

[72] S.N. Habisreutinger, L. Schmidt-Mende, J.K. Stolarczyk, Photocatalytic reduction of CO_2 on TiO_2 and other semiconductors, Angew. Chemie - Int. Ed. 52 (2013) 7372–7408. https://doi.org/10.1002/anie.201207199.

[73] D. Shi, Y. Feng, S. Zhong, Photocatalytic conversion of CH_4 and CO_2 to oxygenated compounds over Cu/CdS-TiO_2/SiO_2 catalyst, in: Catal. Today, 2004: pp. 505–509. https://doi.org/10.1016/j.cattod.2004.09.004.

[74] L. Yuliati, H. Itoh, H. Yoshida, Photocatalytic conversion of methane and carbon dioxide over gallium oxide, Chem. Phys. Lett. 452 (2008) 178–182. https://doi.org/10.1016/j.cplett.2007.12.051.

[75] M. Tahir, B. Tahir, N.S. Amin, Photocatalytic CO_2 reduction by CH_4 over montmorillonite modified TiO_2 nanocomposites in a continuous monolith photoreactor, Mater. Res. Bull. 63 (2015) 13–23. https://doi.org/10.1016/j.materresbull.2014.11.042.

[76] M. Tahir, B. Tahir, Z.Y. Zakaria, A. Muhammad, Enhanced photocatalytic carbon dioxide reforming of methane to fuels over nickel and montmorillonite supported TiO_2 nanocomposite under UV-light using monolith photoreactor, J. Clean. Prod. 213 (2019) 451–461. https://doi.org/10.1016/j.jclepro.2018.12.169.

[77] M.U. Azam, M. Tahir, M. Umer, M.M. Jaffar, M.G.M. Nawawi, Engineering approach to enhance photocatalytic water splitting for dynamic H_2 production using La_2O_3/TiO_2 nanocatalyst in a monolith photoreactor, Appl. Surf. Sci. 484 (2019) 1089–1101. https://doi.org/10.1016/j.apsusc.2019.04.030.

[78] B. Tahir, M. Tahir, N.A.S. Amin, Photocatalytic carbon dioxide and methane reduction to fuels over la-promoted titanium dioxide nanocatalyst, Chem. Eng. Trans. 56 (2017) 1123–1128. https://doi.org/10.3303/CET1756188.

[79] B. Han, W. Wei, L. Chang, P. Cheng, Y.H. Hu, Efficient Visible Light Photocatalytic CO_2 Reforming of CH_4, ACS Catal. 6 (2016) 494–497. https://doi.org/10.1021/acscatal.5b02653.

[80] A. Muhammad, M. Tahir, S.S. Al-Shahrani, A. Mahmood Ali, S.U. Rather, Template free synthesis of graphitic carbon nitride nanotubes mediated by lanthanum (La/g-CNT) for selective photocatalytic CO_2 reduction via dry reforming of methane (DRM) to fuels, Appl. Surf. Sci. 504 (2020) 144177. https://doi.org/10.1016/j.apsusc.2019.144177.

[81] B. Tahir, M. Tahir, N.A.S. Amin, Photo-induced CO_2 reduction by CH_4 /H_2O to fuels over Cu-modified g-C_3N_4 nanorods under simulated solar energy, Appl. Surf. Sci. 419 (2017) 875–885. https://doi.org/10.1016/j.apsusc.2017.05.117.

[82] N. Li, Y. Li, R. Jiang, J. Zhou, M. Liu, Photocatalytic coupling of methane and CO_2 into C_2-hydrocarbons over Zn doped g-C_3N_4 catalysts, Appl. Surf. Sci. 498 (2019) 143861. https://doi.org/10.1016/j.apsusc.2019.143861.

[83] H. Liu, T.D. Dao, L. Liu, X. Meng, T. Nagao, J. Ye, Light assisted CO_2 reduction with methane over group VIII metals: Universality of metal localized surface plasmon resonance in reactant activation, Appl. Catal. B Environ. 209 (2017) 183–189. https://doi.org/10.1016/j.apcatb.2017.02.080.

[84] Q. Zhang, M. Mao, Y. Li, Y. Yang, H. Huang, Z. Jiang, Q. Hu, S. Wu, X. Zhao, Novel photoactivation promoted light-driven CO_2 reduction by CH_4 on Ni/CeO_2 nanocomposite with high light-to-fuel efficiency and enhanced stability, Appl. Catal. B Environ. 239 (2018) 555–564. https://doi.org/10.1016/j.apcatb.2018.08.052.

[85] D. Takami, Y. Ito, S. Kawaharasaki, A. Yamamoto, H. Yoshida, Low temperature dry reforming of methane over plasmonic Ni photocatalysts under visible light irradiation, Sustain. Energy Fuels. 3 (2019) 2968–2971. https://doi.org/10.1039/c9se00206e.

[86] H. Liu, M. Li, T.D. Dao, Y. Liu, W. Zhou, L. Liu, X. Meng, T. Nagao, J. Ye, Design of PdAu alloy plasmonic nanoparticles for improved catalytic performance in CO_2 reduction with visible light irradiation, Nano Energy. 26 (2016) 398–404. https://doi.org/10.1016/j.nanoen.2016.05.045.

[87] H. Song, X. Meng, T.D. Dao, W. Zhou, H. Liu, L. Shi, H. Zhang, T. Nagao, T. Kako, J. Ye, Light-Enhanced Carbon Dioxide Activation and Conversion by Effective Plasmonic Coupling Effect of Pt and Au Nanoparticles, ACS Appl. Mater. Interfaces. 10 (2018) 408–416. https://doi.org/10.1021/acsami.7b13043.

[88] L. Zhou, J.M.P. Martirez, J. Finzel, C. Zhang, D.F. Swearer, S. Tian, H. Robatjazi, M. Lou, L. Dong, L. Henderson, P. Christopher, E.A. Carter, P. Nordlander, N.J. Halas, Light-driven methane dry reforming with single atomic site antenna-reactor plasmonic photocatalysts, Nat. Energy. 5 (2020) 61–70. https://doi.org/10.1038/s41560-019-0517-9.

[89] Á. Kukovecz, K. Kordás, J. Kiss, Z. Kónya, Atomic scale characterization and surface chemistry of metal modified titanate nanotubes and nanowires, Surf. Sci. Rep. 71 (2016) 473–546. https://doi.org/10.1016/j.surfrep.2016.06.001.

[90] B. László, K. Baán, A. Oszkó, A. Erdőhelyi, J. Kiss, Z. Kónya, Hydrogen evolution in the photocatalytic reaction between methane and water in the presence of CO_2 on titanate and titania supported Rh and Au catalysts, Top. Catal. 61 (2018) 875–888. https://doi.org/10.1007/s11244-018-0936-z.

[91] N.M. Dimitrijevic, B.K. Vijayan, O.G. Poluektov, T. Rajh, K.A. Gray, H. He, P. Zapol, Role of water and carbonates in photocatalytic transformation of CO_2 to CH_4 on titania,

J. Am. Chem. Soc. 133 (2011) 3964–3971. https://doi.org/10.1021/ja108791u.

[92] H. Yoshida, K. Hirao, J.I. Nishimoto, K. Shimura, S. Kato, H. Itoh, T. Hattori, Hydrogen production from methane and water on platinum loaded titanium oxide photocatalysts, J. Phys. Chem. C. 112 (2008) 5542–5551. https://doi.org/10.1021/jp077314u.

[93] K. Shimura, T. Yoshida, H. Yoshida, Photocatalytic activation of water and methane over modified gallium oxide for hydrogen production, J. Phys. Chem. C. 114 (2010) 11466–11474. https://doi.org/10.1021/jp1012126.

[94] H. Yoshida, S. Kato, K. Hirao, J.I. Nishimoto, T. Hattori, Photocatalytic steam reforming of methane over platinum-loaded semiconductors for hydrogen production, Chem. Lett. 36 (2007) 430–431. https://doi.org/10.1246/cl.2007.430.

[95] K. Shimura, S. Kato, T. Yoshida, H. Itoh, T. Hattori, H. Yoshida, Photocatalytic steam reforming of methane over sodium tantalate, J. Phys. Chem. C. 114 (2010) 3493–3503. https://doi.org/10.1021/jp902761x.

[96] L. Yu, Y. Shao, D. Li, Direct combination of hydrogen evolution from water and methane conversion in a photocatalytic system over Pt/TiO_2, Appl. Catal. B Environ. 204 (2017) 216–223. https://doi.org/10.1016/j.apcatb.2016.11.039.

[97] K. Shimura, H. Kawai, T. Yoshida, H. Yoshida, Bifunctional rhodium cocatalysts for photocatalytic steam reforming of methane over alkaline titanate, ACS Catal. 2 (2012) 2126–2134. https://doi.org/10.1021/cs2006229.

[98] B. Tahir, M. Tahir, N.A.S. Amin, Silver loaded protonated graphitic carbon nitride ($Ag/pg\text{-}C_3N_4$) nanosheets for stimulating CO_2 reduction to fuels via photocatalytic bi-reforming of methane, Appl. Surf. Sci. 493 (2019) 18–31. https://doi.org/10.1016/j.apsusc.2019.06.257.

[99] K. Okabe, K. Sayama, H. Kusama, H. Arakawa, Photo-oxidative coupling of methane

over TiO_2-based catalysts, Chem. Lett. (1997) 457–458. https://doi.org/10.1246/cl.1997.457.

[100] G.N. Kuzmin, M. V. Knatko, S. V. Kurganov, Light and X-ray-induced chemistry of methane on TiO_2, React. Kinet. Catal. Lett. 23 (1983) 313–317. https://doi.org/10.1007/BF02065581.

[101] L. Yuliati, T. Hattori, H. Itoh, H. Yoshida, Photocatalytic nonoxidative coupling of methane on gallium oxide and silica-supported gallium oxide, J. Catal. 257 (2008) 396–402. https://doi.org/10.1016/j.jcat.2008.05.022.

[102] L. Yuliati, M. Tsubota, A. Satsuma, H. Itoh, H. Yoshida, Photoactive sites on pure silica materials for nonoxidative direct methane coupling, J. Catal. 238 (2006) 214–220. https://doi.org/10.1016/j.jcat.2005.12.002.

[103] H. Yoshida, N. Matsushita, Y. Kato, T. Hattori, Synergistic active sites on SiO_2-Al_2O_3-TiO_2 photocatalysts for direct methane coupling, J. Phys. Chem. B. 107 (2003) 8355–8362. https://doi.org/10.1021/jp034458+.

[104] L. Yuliati, T. Hamajima, T. Hattori, H. Yoshida, Highly dispersed Ce(III) species on silica and alumina as new photocatalysts for non-oxidative direct methane coupling, Chem. Commun. (2005) 4824–4826. https://doi.org/10.1039/b507698f.

[105] H. Yoshida, M.G. Chaskar, Y. Kato, T. Hattori, Active sites on silica-supported zirconium oxide for photoinduced direct methane conversion and photoluminescence, J. Photochem. Photobiol. A Chem. 160 (2003) 47–53. https://doi.org/10.1016/S1010-6030(03)00220-X.

[106] L. Li, G.D. Li, C. Yan, X.Y. Mu, X.L. Pan, X.X. Zou, K.X. Wang, J.S. Chen, Efficient sunlight-driven dehydrogenative coupling of methane to ethane over a Zn^+-modified zeolite, Angew. Chemie - Int. Ed. 50 (2011) 8299–8303. https://doi.org/10.1002/anie.201102320.

[107] L. Meng, Z. Chen, Z. Ma, S. He, Y. Hou, H.H. Li, R. Yuan, X.H. Huang, X. Wang, X. Wang, J. Long, Gold plasmon-induced photocatalytic dehydrogenative coupling of methane to ethane on polar oxide surfaces, Energy Environ. Sci. 11 (2018) 294–298. https://doi.org/10.1039/c7ee02951a.

[108] N. Li, R. Jiang, Y. Li, J. Zhou, Q. Ma, S. Shen, M. Liu, Plasma-Assisted Photocatalysis of CH_4 and CO_2 into Ethylene, ACS Sustain. Chem. Eng. 7 (2019) 11455–11463. https://doi.org/10.1021/acssuschemeng.9b01284.

[109] X. Li, J. Xie, H. Rao, C. Wang, J. Tang, Platinum- and CuO_x-Decorated TiO_2 Photocatalyst for Oxidative Coupling of Methane to C_2 Hydrocarbons in a Flow Reactor, Angew. Chemie - Int. Ed. (2020) 1–7. https://doi.org/10.1002/anie.202007557.

[110] X. Yu, V.L. Zholobenko, S. Moldovan, D. Hu, D. Wu, V. V Ordomsky, A.Y. Khodakov, Stoichiometric methane conversion to ethane using photochemical looping at ambient temperature, Nat. Energy. (2020). https://doi.org/10.1038/s41560-020-0616-7.

[111] A. Hu, J.J. Guo, H. Pan, Z. Zuo, Selective functionalization of methane, ethane, and higher alkanes by cerium photocatalysis, Science 361 (2018) 668–672. https://doi.org/10.1126/science.aat9750.

[112] L. Li, S. Fan, X. Mu, Z. Mi, C.J. Li, Photoinduced conversion of methane into benzene over GaN nanowires, J. Am. Chem. Soc. 136 (2014) 7793–7796. https://doi.org/10.1021/ja5004119.

[113] X. Guo, G. Fang, G. Li, H. Ma, H. Fan, L. Yu, C. Ma, X. Wu, D. Deng, M. Wei, D. Tan, R. Si, S. Zhang, J. Li, L. Sun, Z. Tang, X. Pan, X. Bao, Direct, nonoxidative conversion of methane to ethylene, aromatics, and hydrogen, Science 344 (2014) 616–619. https://doi.org/10.1126/science.1253150.

[114] H. Huang, M. Mao, Q. Zhang, Y. Li, J. Bai, Y. Yang, M. Zeng, X. Zhao, Solar-Light-Driven CO_2 Reduction by CH_4 on Silica-Cluster-Modified Ni Nanocrystals with a High Solar-to-Fuel Efficiency and Excellent Durability, Adv. Energy Mater. 8 (2018) 1–11. https://doi.org/10.1002/aenm.201702472.

[115] H. Song, X. Meng, S. Wang, W. Zhou, X. Wang, T. Kako, J. Ye, Direct and Selective Photocatalytic Oxidation of CH_4 to Oxygenates with O_2 on Cocatalysts/ZnO at Room Temperature in Water, J. Am. Chem. Soc. 141 (2019) 20507–20515. https://doi.org/10.1021/jacs.9b11440.

[116] Y. Zhou, L. Zhang, W. Wang, Direct functionalization of methane into ethanol over copper modified polymeric carbon nitride via photocatalysis, Nat. Commun. 10 (2019) 1–8. https://doi.org/10.1038/s41467-019-08454-0.

[117] L. Li, S. Fan, X. Mu, Z. Mi, C.J. Li, Photoinduced conversion of methane into benzene over GaN nanowires, J. Am. Chem. Soc. 136 (2014) 7793–7796. https://doi.org/10.1021/ja5004119.

[118] A.A. Khan, M. Tahir, Recent advancements in engineering approach towards design of photo-reactors for selective photocatalytic CO_2 reduction to renewable fuels, J. CO_2 Util. 29 (2019) 205–239. https://doi.org/10.1016/j.jcou.2018.12.008.

[119] P.Y. Liou, S.C. Chen, J.C.S. Wu, D. Liu, S. MacKintosh, M. Maroto-Valer, R. Linforth, Photocatalytic CO_2 reduction using an internally illuminated monolith photoreactor, Energy Environ. Sci. 4 (2011) 1487–1494. https://doi.org/10.1039/c0ee00609b.

[120] O. Ola, M.M. Maroto-Valer, Review of material design and reactor engineering on TiO_2 photocatalysis for CO_2 reduction, J. Photochem. Photobiol. C Photochem. Rev. 24 (2015) 16–42. https://doi.org/10.1016/j.jphotochemrev.2015.06.001.

[121] V.H. Nguyen, J.C.S. Wu, Recent developments in the design of photoreactors for solar

energy conversion from water splitting and CO_2 reduction, Appl. Catal. A Gen. 550 (2018) 122–141. https://doi.org/10.1016/j.apcata.2017.11.002.

[122] S. Xie, S. Lin, Q. Zhang, Z. Tian, Y. Wang, Selective electrocatalytic conversion of methane to fuels and chemicals, J. Energy Chem. 27 (2018) 1629–1636. https://doi.org/10.1016/j.jechem.2018.03.015.

[123] A. Hassan, B. Mostaghimi, T.A. Al-Attas, M. Golam Kibria, S. Siahrostami, A review on electrocatalytic oxidation of methane to oxygenates, (2020). https://doi.org/10.1039/d0ta03758c.

[124] N. Spinner, W.E. Mustain, Electrochemical Methane Activation and Conversion to Oxygenates at Room Temperature, ECS Trans. 53 (2013) 1–20. https://doi.org/10.1149/05323.0001ecst.